Searches for beyond-the-standard model physics in events with a Z boson, jets and missing transverse energy

D. Barge, C. Campagnari, D. Kovalskyi, V. Krutelyov

University of California, Santa Barbara, USA

W. Andrews, G. Cerati, D. Evans, F. Golf, I. MacNeill, S. Padhi, Y. Tu, F. Würthwein, A. Yagil, J. Yoo

University of California, San Diego, USA

L. Bauerdick, K. Burkett, I. Fisk, Y. Gao, O. Gutsche, B. Hooberman, S. Jindariani, J. Linacre, V. Martinez Outschoorn

Fermi National Accelerator Laboratory, Batavia, Illinois, USA

Abstract

This note describes a search for beyond-the-standard model (BSM) physics in events with a leptonically-decaying Z boson, jets, and missing transverse energy (E_T^{miss}). This signature is predicted to occur in several BSM scenarios, for example supersymmetric (SUSY) models. Two search strategies are pursued. The first is an inclusive approach which selects events with at least two jets and large E_T^{miss}, produced in association with the $Z \to \ell\ell$ candidate. The second is a targeted search in which additional requirements are imposed in order to achieve sensitivity to the production of the weakly-coupled SUSY charginos and neutralinos. The main backgrounds of SM $Z + \text{jets}$ and $t\bar{t}$ production are estimated with the data-driven E_T^{miss} templates technique and the opposite-flavor subtraction technique, respectively Additional backgrounds are estimated from simulation after validation in data control samples. Good agreement is observed between the data and the predicted background in low E_T^{miss} control regions, which validates the background estimation methodology. The results in the signal regions, defined by the requirement $E_T^{miss} > 100$ GeV, will be unblinded soon. These results will be interpreted in the context of simplified model spectra.

Contents

1 Changes w.r.t. previous AN Version

- v2: Update to 9.2 fb^{-1} of 53X data and MC (v1 used 5.1 fb^{-1} 52X data and MC).

2 Introduction

This note presents two searches for beyond-the-standard model (BSM) physics in events containing a leptonically-decaying Z boson, jets, and missing transverse energy. This is an update of previous searches performed with 2011 data [1, 2]. The search is based on a data sample of pp collisions collected at $\sqrt{s} = 8$ TeV in 2012, corresponding to an integrated luminosity of 9.2 fb^{-1}.

The production of Z bosons is expected in many BSM scenarios, for example supersymmetric (SUSY) models. In SUSY models with neutralino lightest SUSY particle (LSP), Z bosons may be produced in the decays $\chi_2^0 \to Z\chi_1^0$, where χ_2^0 is the second lightest neutralino and χ_1^0 is the lightest neutralino. In models with gravitino LSP such as gauge-mediated SUSY breaking (GMSB) models, Z bosons may be produced via $\chi_1^0 \to Z\tilde{G}$, where $\tilde{G}$ is the gravitino. Such decays may occur either in the cascade decays of the strongly-produced squarks and gluinos, or via direct production of the electroweak charginos and neutralino. Examples of such processes (see Fig. 1) are:

- strong production: $pp \to \tilde{g}\tilde{g} \to (q\bar{q}\chi_2^0)(q\bar{q}\chi_2^0) \to (q\bar{q}Z\chi_1^0)(q\bar{q}Z\chi_1^0) \to ZZ + 4$ jets $+ E_T^{miss}$

- electroweak production: $pp \to \chi_1^\pm \chi_2^0 \to (W\chi_1^0)(Z\chi_1^0) \to WZ + E_T^{miss}$
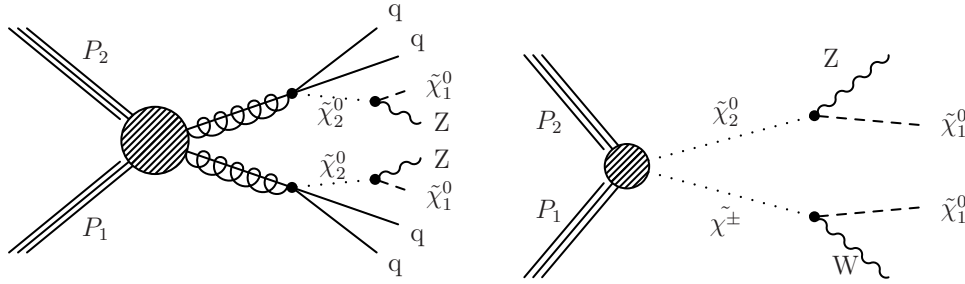

Figure 1: Examples of BSM physics signatures targeted in this search. In the left diagram, Z bosons are produced in the cascade decays of the strongly-interacting gluinos. In the right diagram, a Z boson is produced via direct production of the weakly-coupled charginos and neutralinos.

We thus pursue two strategies. The first is an inclusive strategy which selects events with a $Z \to \ell\ell$ candidate, at least two jets, and large E_T^{miss}. This strategy is useful for targeting, e.g., the production of Z bosons in the cascade decays of strongly-interacting particles as depicted in Fig. 1 (left). In the second strategy, we impose additional requirements which strongly suppress the backgrounds while retaining high efficiency for events with Z bosons produced via direct production of the weakly-coupled charginos and neutralinos. These two strategies are referred to as the "inclusive search" and the "targeted search," respectively.

After selecting events with jets and a $Z \to \ell^+\ell^-$ ($\ell = e, \mu$) candidate, the dominant background consists of SM Z production accompanied by jets from initial-state radiation ($Z +$ jets). The E_T^{miss} in $Z +$ jets events arises primarily when jet energies are mismeasured. The $Z +$ jets cross section is several orders of magnitude larger than our signal, and the artificial E_T^{miss} is not necessarily well reproduced in simulation. Therefore, the critical prerequisite to a discovery of BSM physics in the $Z +$ jets $+ E_T^{miss}$ final state is to establish that a potential excess is not due to SM $Z +$ jets production accompanied by artificial E_T^{miss} from jet mismeasurements. In this note, the $Z +$ jets background is estimated with the E_T^{miss} templates technique, in which the artificial E_T^{miss} in $Z +$ jets events is modeled using a $\gamma +$ jets control sample. The second background category consists of processes which produce leptons with uncorrelated flavor. These "flavor-symmetric" (FS) backgrounds, which are dominated by $t\bar{t}$ but also contain WW, DY$\to \tau\tau$ and single top processes, are estimated using a data control sample of eμ events. Additional backgrounds from WZ and ZZ production are estimated from MC, after validation of the MC modeling of these processes using 3-lepton and 4-lepton data control samples.

3 Datasets and Triggers

In this section we list the datasets, triggers, and MC samples used in the analysis. For selecting signal events, we use dilepton triggers in the DoubleElectron, DoubleMu, and MuEG datasets. An event in the ee final state is required to pass the dielectron trigger, a $\mu\mu$ event is required to pass the dimuon trigger, while an eμ event is required to pass at least one of the two $e - \mu$ cross triggers. The efficiencies of the ee, $\mu\mu$ and eμ triggers with respect to the offline selection have been measured as 0.95 ± 0.03, 0.88 ± 0.03, and 0.92 ± 0.03, respectively [6]. These trigger efficiencies were measured with the first 5.1 fb^{-1} and will be updated with the full data sample. Preliminary measurements of the trigger efficiency with the full sample show consistent results within $\sim 1 - 2\%$. A sample of $\gamma+$jets events, used as a control sample to estimate the $Z+$jets background, is selected using a set of single photon triggers. The golden json of Aug 31st, corresponding to an integrated luminosity of 9.7 fb^{-1}, is used as the starting point. However, due to a bug in the Run2012C-PromptReco-v1 data samples (corresponding to 0.5 fb^{-1}), this portion of the data is currently excluded but will be added back after it is reprocessed. Thus we currently use a sample corresponding to 9.2 fb^{-1}. All data and MC samples are processed in CMSSW_5_3_2_patch4.

- Datasets

  - /DoubleElectron/Run2012A-13Jul2012-v1/AOD

  - /DoubleMu/Run2012A-13Jul2012-v1/AOD

  - /MuEG/Run2012A-13Jul2012-v1/AOD

  - /DoubleElectron/Run2012B-13Jul2012-v1/AOD

  - /DoubleMu/Run2012B-13Jul2012-v1/AOD

  - /MuEG/Run2012B-13Jul2012-v1/AOD

  - /DoubleElectron/Run2012C-PromptReco-v2/AOD

  - /DoubleMu/Run2012C-PromptReco-v2/AOD

  - /MuEG/Run2012C-PromptReco-v2/AOD

- Triggers

  - HLT_Mu17_Mu8_v*

  - HLT_Mu17_Ele8_CaloIdT_CaloIsoVL_TrkIdVL_TrkIsoVL_v*

  - HLT_Mu8_Ele17_CaloIdT_CaloIsoVL_TrkIdVL_TrkIsoVL*

  - HLT_Ele17_CaloIdT_CaloIsoVL_TrkIdVL_TrkIsoVL_Ele8_CaloIdT_CaloIsoVL_TrkIdVL_TrkIsoVL_v*

  - HLT_Photon22_R9Id90_HE10_Iso40_EBOnly_v*

  - HLT_Photon36_R9Id90_HE10_Iso40_EBOnly_v*

  - HLT_Photon50_R9Id90_HE10_Iso40_EBOnly_v*

  - HLT_Photon75_R9Id90_HE10_Iso40_EBOnly_v*

  - HLT_Photon90_R9Id90_HE10_Iso40_EBOnly_v*

Table 1: List of MC samples.

Process	Dataset Name	Cross Section [pb]
$Z +$ jets	/DYJetsToLL_M-50_TuneZ2Star_8TeV-madgraph-tarball/Summer12_DR53X-PU_S10_START53_V7A-v1/AODSIM	3532.8
$t\bar{t}$	/TTJets_MassiveBinDECAY_TuneZ2star_8TeV-madgraph-tauola/Summer12_DR53X-PU_S10_START53_V7A-v1/AODSIM	225.2
ZZ	/ZZJetsTo4L_TuneZ2star_8TeV-madgraph-tauola/Summer12_DR53X-PU_S10_START53_V7A-v1/AODSIM	0.1769
	/ZZJetsTo2L2Q_TuneZ2star_8TeV-madgraph-tauola/Summer12_DR53X-PU_S10_START53_V7A-v1/AODSIM	2.4487
	/ZZJetsTo2L2Nu_TuneZ2star_8TeV-madgraph-tauola/Summer12_DR53X-PU_S10_START53_V7A-v3/AODSIM	0.3648
WZ	/WZJetsTo3LNu_TuneZ2_8TeV-madgraph-tauola/Summer12_DR53X-PU_S10_START53_V7A-v1/AODSIM	1.0575
	/WZJetsTo2L2Q_TuneZ2star_8TeV-madgraph-tauola/Summer12_DR53X-PU_S10_START53_V7A-v1/AODSIM	2.206
WW	/WWJetsTo2L2Nu_TuneZ2star_8TeV-madgraph-tauola/Summer12_DR53X-PU_S10_START53_V7A-v1/AODSIM	5.8123
single top	/T_tW-channel-DR_TuneZ2star_8TeV-powheg-tauola/Summer12_DR53X-PU_S10_START53_V7A-v1/AODSIM	11.177
	/Tbar_tW-channel-DR_TuneZ2star_8TeV-powheg-tauola/Summer12_DR53X-PU_S10_START53_V7A-v1/AODSIM	11.177
ttV	/TTZJets_8TeV-madgraph_v2/Summer12_DR53X-PU_S10_START53_V7A-v1/AODSIM	0.208
	/TTWJets_8TeV-madgraph/Summer12_DR53X-PU_S10_START53_V7A-v1/AODSIM	0.232
VVV	/ZZZNoGstarJets_8TeV-madgraph/Summer12_DR53X-PU_S10_START53_V7A-v1/AODSIM	0.01922
	/WWWJets_8TeV-madgraph/Summer12_DR53X-PU_S10_START53_V7A-v1/AODSIM	0.08217
	/WWZNoGstarJets_8TeV-madgraph/Summer12_DR53X-PU_S10_START53_V7A-v1/AODSIM	0.0633

4 Selection

In this section, we list the event selection, electron and muon objects selections, jets, E_T^{miss}, and b-tagging selections used in this analysis. These selections are based on those recommended by the relevant POG's.

4.1 Event Selection

We require the presence of at least one primary vertex satisfying the standard quality criteria; namely, vertex is not fake, $\text{ndf} \geq 4$, $\rho < 2$ cm, and $|z| < 24$ cm.

4.2 Lepton Selection

Because $Z \to \ell\ell$ ($\ell = e, \mu$) is a final state with very little background, we restrict ourselves to events in which the Z boson decays to electrons or muons only. Therefore opposite sign leptons passing the identification and isolation requirements described below are required in each event.

- $p_T > 20$ GeV and $|\eta| < 2.4$;

- Opposite-sign same-flavor (SF) ee and $\mu\mu$ lepton pairs (opposite-flavor (OF) eμ lepton pairs are retained in a control sample used to estimate the FS contribution);

- For SF events, the dilepton invariant mass is required to be consistent with the Z mass; namely $81 < m_{\ell\ell} < 101$ GeV.

4.2.1 Electron Selection

The electron selection is the loose working point recommended by the E/gamma POG, as documented at [3]. Electrons with $p_T > 20$ GeV and $|\eta| < 2.4$ are considered. We use PF-based isolation with a cone size of $\Delta R < 0.3$, using the effective area rho corrections documented at [4], and we require a relative isolation < 0.15. Electrons in the transition region defined by $1.4442 < |\eta_{SC}| < 1.566$ are rejected. Electrons with a selected muon with $p_T > 10$ GeV within $\Delta R < 0.1$ are rejected. The electron selection requirements are listed in Table 2 for completeness.

Table 2: Summary of the electron selection requirements.

Quantity	Barrel	Endcap
$\delta\eta$	< 0.007	< 0.009
$\delta\phi$	< 0.15	< 0.10
$\sigma_{i\eta i\eta}$	< 0.01	< 0.03
H/E	< 0.12	< 0.10
d_0 (w.r.t. 1st good PV)	< 0.02 cm	< 0.02 cm
d_z (w.r.t. 1st good PV)	< 0.2 cm	< 0.2 cm
$|1/E - 1/P|$	$< 0.05\,\text{GeV}^{-1}$	$< 0.05\,\text{GeV}^{-1}$
PF isolation / p_T	< 0.15	< 0.15
conversion rejection: fit probability	$< 10^{-6}$	$< 10^{-6}$
conversion rejection: missing hits	≤ 1	≤ 1

4.2.2 Muon Selection

We use the tight muon selection recommended by the muon POG, as documented at [5]. Muons with $p_T > 20$ GeV and $|\eta| < 2.4$ are considered. We use PF-based isolation with a cone size of $\Delta R < 0.3$, using the $\Delta\beta$ PU correction scheme, and we require a relative isolation of < 0.15. The muon selection requirements are listed in Table 3 for completeness.

4.2.3 PF Leptons

For consistency with pfmet, both electrons and muons are required to be reconstructed as PF electrons and PF muons, respectively, with $p_T > 20$ GeV. For defining the dilepton invariant mass, the 4-momenta of the PF leptons are used.

Table 3: Summary of the muons selection requirements.

Quantity	Requirement
muon type	global muon and PF muon
χ^2/ndf	< 10
muon chamber hits	≥ 1
matched stations	≥ 2
d_0 (w.r.t. 1st good PV)	< 0.02 cm
d_z (w.r.t. 1st good PV)	< 0.5 cm
pixel hits	≥ 1
tracker layers	≥ 5

4.3 Photons

As will be explained later, it is not essential that we select real photons. What is needed are jets that are predominantly electromagnetic, well measured in the ECAL, and hence less likely to contribute to fake MET. We select photons with:

- $p_T > 22$ GeV

- $|\eta| < 2$

- $H/E < 0.1$

- No matching pixel track (pixel veto)

- There must be a pfjet of $p_T > 10$ GeV matched to the photon within $dR < 0.3$. The matched jet is required to have a neutral electromagnetic energy fraction of at least 70%.

- We require that the pfjet p_T matched to the photon satisfy (pfjet p_T - photon p_T) > -5 GeV. This removes a few rare cases in which "overcleaning" of a pfjet generates fake MET.

- We also match photons to calojets and require (calojet p_T - photon p_T) > -5 GeV (the same requirement used for pfjets). This is to remove other rare cases in which fake energy is added to the photon object but not the calojet.

- We reject photons which have an electron of at least $p_T > 10$ GeV within $dR < 0.2$ in order to reject conversions from electrons from W decays which are accompanied by real MET.

- We reject photons which are aligned with the MET to within 0.14 radians in phi.

4.4 MET

We use pfmet, henceforth referred to simply as $\mathrm{E_T^{miss}}$.

4.5 Jets

- PF jets with L1FastL2L3 corrections (MC), L1FastL2L3residual corrections (data), using the 52X jet energy corrections

- $|\eta| < 2.5$

- Passes loose PFJet ID

- $p_T > 30$ GeV for determining the jet multiplicity, $p_T > 15$ GeV for calculation of H_T

- For the creation of photon templates, the jet matched to the photon passing the photon selection described above is vetoed

- For the dilepton sample, jets are vetoed if they are within $\Delta R < 0.4$ from any lepton $p_T > 20$ GeV passing analysis selection

5   Data vs. MC Comparison in Preselection Region

In this section we compare the data and MC samples passing the selection described in Sec. 4 In the following, the MC is reweighted to match the data distribution of number of reconstructed primary vertices. The trigger efficiencies of Sec. 3 are applied. In all plots, the last bin contains the overflow.

We begin by counting the inclusive Z yields. Here we require the presence of two selected leptons without any additional requirements on jets or E_T^{miss}. In Fig. 2 the distribution of dilepton invariant mass in the ee and $\mu\mu$ channels is displayed. In Table 4 the yields for selected dilepton events in the Z mass window are indicated. Good data vs. MC agreement is observed, within the systematic uncertainties of integrated luminosity (4.5%), trigger efficiency (3%), $Z + \text{jets}$ and $t\bar{t}$ cross sections.
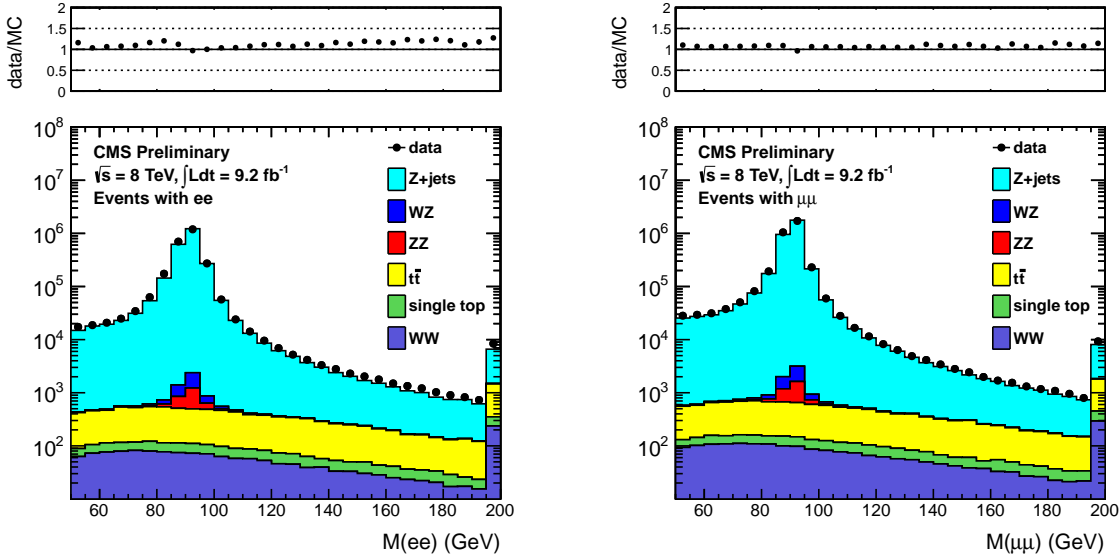

Figure 2: Dilepton mass distribution for events with two selected leptons in the ee (left) and $\mu\mu$ (right) final states.

Table 4: Data and Monte Carlo yields for events with two selected leptons in the Z mass window.

Sample	ee	$\mu\mu$	eμ	total
$Z + \text{jets}$	22662501 ± 1660	3125059 ± 1873	1082 ± 35.8	5392392 ± 2503
$t\bar{t}$	1579.1 ± 22.6	1998.3 ± 24.4	3592.2 ± 33.5	7169.5 ± 47.2
WW	290.6 ± 2.9	387.2 ± 3.3	671.2 ± 4.4	1349.0 ± 6.2
WZ	2052.6 ± 3.6	2686.9 ± 3.9	54.1 ± 0.5	4793.5 ± 5.3
ZZ	1294.6 ± 2.7	1708.5 ± 3.0	5.2 ± 0.1	3008.3 ± 4.0
single top	150.0 ± 5.9	192.6 ± 6.4	332.9 ± 8.6	675.5 ± 12.2
total SM MC	2271617 ± 1661	3132032 ± 18723	5738 ± 50.0	5409387 ± 2503
data	2329993	3169480	6182	5505655

We next define the preselection region for the inclusive search using the following requirements:

- Number of jets ≥ 2;

- Same flavor dileptons (opposite flavor yields will be shown since they are used in data for the FS background estimation);

- Dilepton invariant mass $81 < m_{\ell\ell} < 101$ GeV.

The dilepton mass distributions in the preselection region of the inclusive search (without the dilepton mass requirement applied) for the ee and $\mu\mu$ final states are shown in Figure 3. In Table 5 the data and MC yields in thepreselection region are indicated. Good data vs. MC agreement is observed.
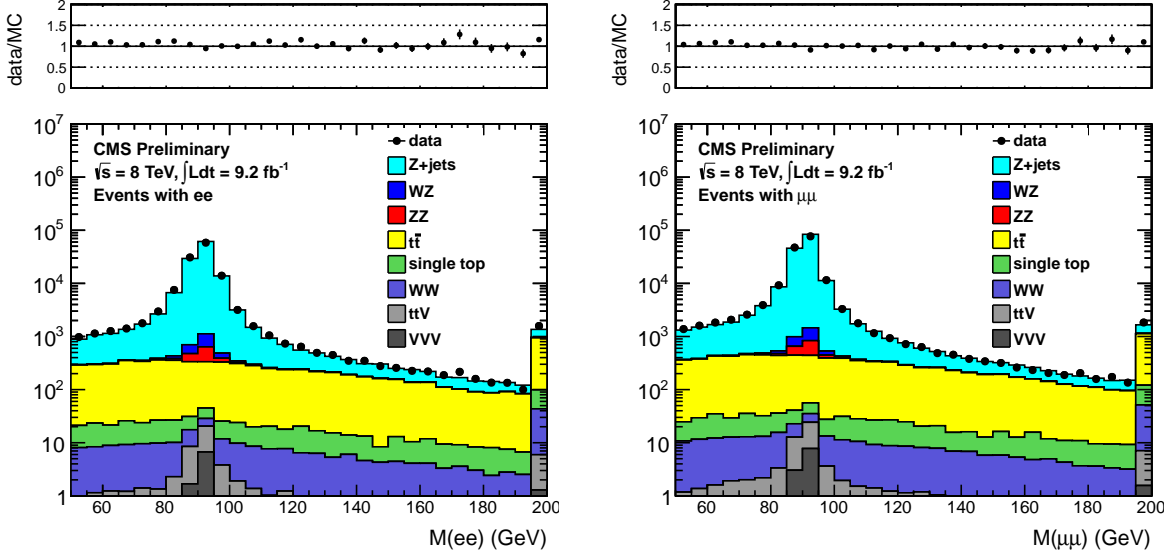

Figure 3: Dilepton mass distribution for events in the preselection region of the inclusive search in the ee (left) and $\mu\mu$ (right) final states.

Table 5: Data and MC yields in the preselection region of the inclusive search.

Sample	ee	$\mu\mu$	eμ	total
Z + jets	108778.2 ± 358.0	145999.4 ± 398.7	59.7 ± 8.3	254837.4 ± 535.9
$t\bar{t}$	1220.9 ± 19.9	1544.7 ± 21.4	2788.1 ± 29.5	5553.8 ± 41.5
WW	32.7 ± 1.0	42.5 ± 1.1	74.7 ± 1.4	149.9 ± 2.0
WZ	853.0 ± 2.4	1100.8 ± 2.6	10.7 ± 0.2	1964.4 ± 3.5
ZZ	532.5 ± 1.8	692.6 ± 2.0	1.2 ± 0.0	1226.3 ± 2.7
single top	60.4 ± 3.7	73.1 ± 3.9	131.8 ± 5.4	265.3 ± 7.6
ttV	25.9 ± 0.5	32.2 ± 0.5	9.4 ± 0.3	67.5 ± 0.8
VVV	9.2 ± 0.1	11.6 ± 0.2	1.6 ± 0.1	22.5 ± 0.2
tot SM MC	111512.9 ± 358.6	149497.0 ± 399.3	3077.2 ± 31.1	264087.1 ± 537.6
data	110325	144122	2966	257413

We next define the preselection region for the targeted search by adding the following requirements:

- Veto events containing a b-tagged jet;

- Dijet invariant mass $70 < m_{jj} < 110$ GeV;

- Veto events containing a third selected lepton (electron or muon) with $p_T > 10$ GeV;

The rejection of events with a b-tagged jet strongly suppresses the $t\bar{t}$ background, which is the dominant background in the inclusive search after requiring large E_T^{miss}. The requirement that the jet pair is consistent with originating from W/Z decay is motivated by the fact that we are searching for signatures producing V(jj)Z($\ell\ell$)+E_T^{miss}; this requirement suppresses the $Z +$ jets and $t\bar{t}$ backgrounds. The veto of events containting a third electron or muon suppresses the WZ background, and also serves to make this analyis exclusive with respect to searches in the trilepton final state.

The dilepton mass distributions in the preselection region of the targeted search (without the dilepton mass requirement applied) for the ee and $\mu\mu$ final states are shown in Figure 4. In Table 6 the data and MC yields in the preselection region are indicated. Good data vs. MC agreement is observed. We also show the distribution of dijet mass in the targeted preselection (with the requirement on this quantity removed) in Fig. 5, which demonstrates that the MC does a reasonable job of modeling this quantity.
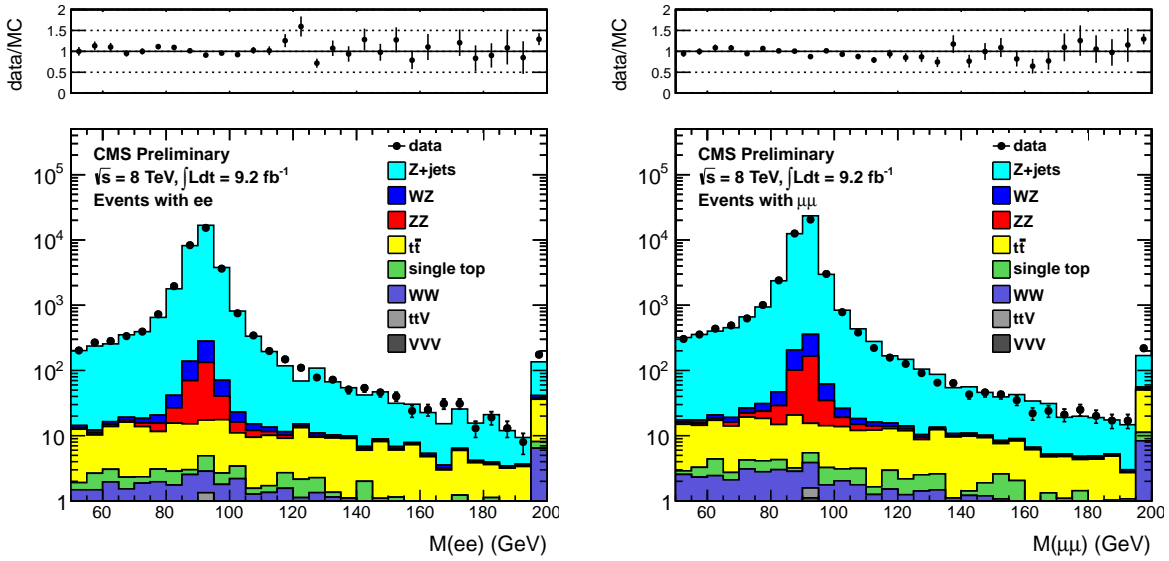

Figure 4: Dilepton mass distribution for events in the preselection region of the targeted search in the ee (left) and $\mu\mu$ (right) final states.

Table 6: Data and MC yields in the preselection region of the targeted search.

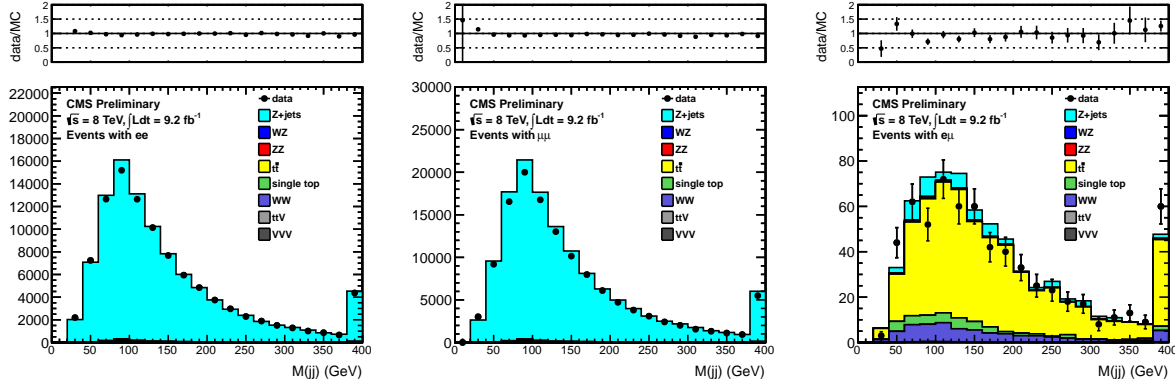| Sample	ee	$\mu\mu$	eμ	total
$Z +$ jets	30033.0 ± 186.9	40552.4 ± 208.9	12.9 ± 3.7	70598.3 ± 280.4
$t\bar{t}$	50.5 ± 4.1	49.1 ± 3.8	105.1 ± 5.7	204.7 ± 8.0
WW	6.8 ± 0.4	8.6 ± 0.5	15.9 ± 0.7	31.3 ± 0.9
WZ	260.7 ± 1.3	339.8 ± 1.4	1.7 ± 0.1	602.2 ± 2.0
ZZ	204.2 ± 1.1	264.0 ± 1.2	0.2 ± 0.0	468.4 ± 1.7
single top	4.7 ± 1.1	5.0 ± 1.0	8.5 ± 1.3	18.2 ± 2.0
ttV	0.7 ± 0.1	0.8 ± 0.1	0.4 ± 0.1	2.0 ± 0.1
VVV	1.4 ± 0.1	1.8 ± 0.1	0.4 ± 0.0	3.6 ± 0.1
tot SM MC	30562.0 ± 187.0	41221.5 ± 208.9	145.2 ± 7.0	71928.6 ± 280.5
data	29183	38388	120	67691

Figure 5: Distributions of dijet mass for the targeted preselection in the ee (left), $\mu\mu$ (middle) and eμ (right) final state.

6 Background Estimation Techniques

In this section we describe the techniques used to estimate the SM backgrounds in our signal regions defined by requirements of large E_T^{miss}. The SM backgrounds fall into three categories:

- $Z + \text{jets}$: this is the dominant background after the preselection. The E_T^{miss} in $Z + \text{jets}$ events is estimated with the "E_T^{miss} templates" technique described in Sec. 6.1;

- Flavor-symmetric (FS) backgrounds: this category includes processes which produces 2 leptons of uncorrelated flavor. It is dominated by $t\bar{t}$ but also contains $Z \to \tau\tau$, WW, and single top processes. This is the dominant contribution in the signal regions, and it is estimated using a data control sample of eμ events as described in Sec. 6.2;

- WZ and ZZ backgrounds: this background is estimated from MC, after validating the MC modeling of these processes using data control samples with jets and exactly 3 leptons (WZ control sample) and exactly 4 leptons (ZZ control sample) as described in Sec. 6.3;

6.1 Estimating the $Z + \text{jets}$ Background with E_T^{miss} Templates

The premise of this data driven technique is that E_T^{miss} in $Z + \text{jets}$ events is produced by the hadronic recoil system and *not* by the leptons making up the Z. Therefore, the basic idea of the E_T^{miss} template method is to measure the E_T^{miss} distribution in a control sample which has no true MET and the same general attributes regarding fake MET as in $Z + \text{jets}$ events. We thus use a sample of $\gamma + \text{jets}$ events, since both $Z + \text{jets}$ and $\gamma + \text{jets}$ events consist of a well-measured object recoiling against hadronic jets.

For selecting photon-like objects, the very loose photon selection described in Sec. 4.3 is used. It is not essential for the photon sample to have high purity. For our purposes, selecting jets with predominantly electromagnetic energy deposition in a good fiducial volume suffices to ensure that they are well measured and do not contribute to fake E_T^{miss}. The $\gamma + \text{jets}$ events are selected with a suite of single photon triggers with p_T thresholds varying from 22–90 GeV. The events are weighted by the trigger prescale such that $\gamma + \text{jets}$ events evenly sample the conditions over the full period of data taking. There remains a small difference in the PU conditions in the $\gamma + \text{jets}$ vs. $Z + \text{jets}$ samples due to the different dependencies of the γ vs. Z isolation efficiencies on PU. To account for this, we reweight the $\gamma + \text{jets}$ samples to match the distribution of reconstructed primary vertices in the $Z + \text{jets}$ sample.

To account for kinematic differences between the hadronic systems in the control vs. signal samples, we measure the E_T^{miss} distributions in the $\gamma + \text{jets}$ sample in bins of the number of jets and the scalar sum of jet transverse energies (H_T). These E_T^{miss} templates are extracted separately from the 5 single photon triggers with thresholds 22, 36, 50, 75, and 90 GeV, so that the templates are effectively binned in photon p_T. All E_T^{miss} distributions are normalized to unit area to form "MET templates". The prediction of the MET in each Z event is the template which corresponds to the N_{jets}, H_T, and Z p_T in the $Z + \text{jets}$ event. The prediction for the Z sample is simply the sum of all such templates. All templates are displayed in App. C.

10

After preselection, there is a small contribution from backgrounds other than $Z + \text{jets}$. To correct for this, the E_T^{miss} templates prediction is scaled such that the total background prediction matches the observed data yield in the E_T^{miss} 0–60 GeV region. Because the non-$Z + \text{jets}$ impurity in the low E_T^{miss} region after preselection is very small, this results in scaling factors of 0.985 (0.995) for the inclusive (targeted) search.

6.2 Estimating the Flavor-Symmetric Background with eμ Events

In this subsection we describe the background estimate for the FS background. Since this background produces equal rates of same-flavor (SF) ee and $\mu\mu$ lepton pairs as opposite-flavor (OF) eμ lepton pairs, the OF yield can be used to estimate the SF yield, after correcting for the different electron vs. muon offline selection efficiencies and the different efficiencies for the ee, $\mu\mu$, and eμ triggers.

An important quantity needed to translate from the OF yield to a prediction for the background in the SF final state is the ratio $R_{\mu e} = \epsilon_\mu / \epsilon_e$, where ϵ_μ (ϵ_e) indicates the offline muon (electron) selection efficiency. This quantity can be extracted from data using the observed $Z \to \mu\mu$ and $Z \to ee$ yields in the preselection region, after correcting for the different trigger efficiencies.

Hence we define:

- $N_{ee}^{\text{trig}} = \epsilon_{ee}^{\text{trig}} N_{ee}^{\text{offline}}$,

- $N_{\mu\mu}^{\text{trig}} = \epsilon_{\mu\mu}^{\text{trig}} N_{\mu\mu}^{\text{offline}}$,

- $N_{e\mu}^{\text{trig}} = \epsilon_{e\mu}^{\text{trig}} N_{e\mu}^{\text{offline}}$.

Here $N_{\ell\ell}^{\text{trig}}$ denotes the number of selected Z events in the $\ell\ell$ channel passing the offline and trigger selection (in other words, the number of recorded and selected events), $\epsilon_{\ell\ell}^{\text{trig}}$ is the trigger efficiency, and $N_{\ell\ell}^{\text{offline}}$ is the number of events that would have passed the offline selection if the trigger had an efficiency of 100%. Thus we calculate the quantity:

$$R_{\mu e} = \sqrt{\frac{N_{\mu\mu}^{\text{offline}}}{N_{ee}^{\text{offline}}}} = \sqrt{\frac{N_{\mu\mu}^{\text{trig}}/\epsilon_{\mu\mu}^{\text{trig}}}{N_{ee}^{\text{trig}}/\epsilon_{ee}^{\text{trig}}}} = \sqrt{\frac{144122/0.88}{110325/0.95}} = 1.19 \pm 0.07. \tag{1}$$

Here we have used the $Z \to \mu\mu$ and $Z \to ee$ yields from Table 5 and the trigger efficiencies quoted in Sec. 3. The indicated uncertainty is due to the 3% uncertainties in the trigger efficiencies. The predicted yields in the ee and $\mu\mu$ final states are calculated from the observed eμ yield as

- $N_{ee}^{\text{predicted}} = \frac{N_{e\mu}^{\text{trig}}}{\epsilon_{e\mu}^{\text{trig}}} \frac{\epsilon_{ee}^{\text{trig}}}{2 R_{\mu e}} = \frac{N_{e\mu}^{\text{trig}}}{0.92} \frac{0.95}{2 \times 1.26} = (0.43 \pm 0.05) \times N_{e\mu}^{\text{trig}}$,

- $N_{\mu\mu}^{\text{predicted}} = \frac{N_{e\mu}^{\text{trig}}}{\epsilon_{e\mu}^{\text{trig}}} \frac{\epsilon_{\mu\mu}^{\text{trig}} R_{\mu e}}{2} = \frac{N_{e\mu}^{\text{trig}}}{0.95} \frac{0.88 \times 1.26}{2} = (0.55 \pm 0.07) \times N_{e\mu}^{\text{trig}}$,

and the predicted yield in the combined ee and $\mu\mu$ channel is simply the sum of these two predictions:

- $N_{ee+\mu\mu}^{\text{predicted}} = (0.99 \pm 0.06) \times N_{e\mu}^{\text{trig}}$.

Note that the relative uncertainty in the combined ee and $\mu\mu$ prediction is smaller than those for the individual ee and $\mu\mu$ predictions because the uncertainty in $R_{\mu e}$ cancels when summing the ee and $\mu\mu$ predictions.

To improve the statistical precision of the FS background estimate, we remove the requirement that the eμ lepton pair falls in the Z mass window. Instead we scale the eμ yield by K, the efficiency for eμ events to satisfy the Z mass requirement, extracted from simulation. In Fig. 6 we display the value of K in data and simulation, for a variety of E_T^{miss} requirements, for the inclusive analysis. Based on this we chose $K = 0.14 \pm 0.02$ for the lower E_T^{miss} regions, $K = 0.14 \pm 0.04$ for the $E_T^{\text{miss}} > 200$ GeV region, and $K = 0.14 \pm 0.09$ for $E_T^{\text{miss}} > 300$ GeV, where the larger uncertainties reflect the reduced statistical precision at large E_T^{miss}. The corresponding plot for the targeted analysis, including the b-veto, is displayed in Fig. 7. Based on this we chose $K = 0.13 \pm 0.02$ for all E_T^{miss} regions up to $E_T^{\text{miss}} > 150$ GeV. For the $E_T^{\text{miss}} > 200$ GeV region we choose $K = 0.13 \pm 0.05$, due to the reduced statistical precision.
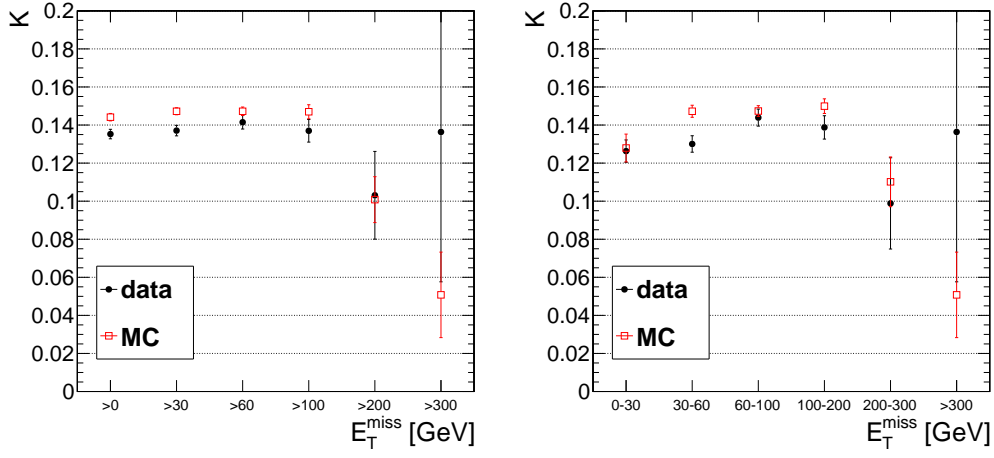
11

Figure 6: The efficiency for eμ events to satisfy the dilepton mass requirement, K, in data and simulation for inclusive E_T^{miss} intervals (left) and exclusive E_T^{miss} intervals (right) for the inclusive analysis.

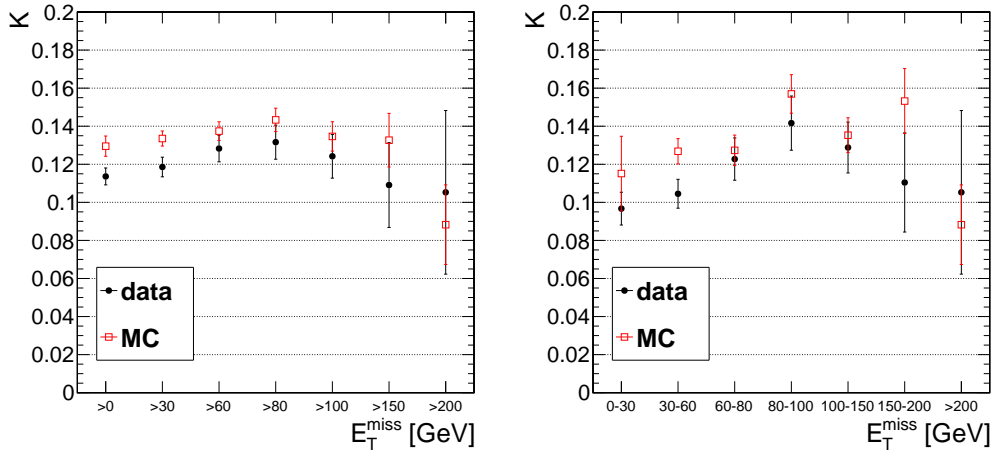

Figure 7: The efficiency for eμ events to satisfy the dilepton mass requirement, K, in data and simulation for inclusive E_T^{miss} intervals (left) and exclusive E_T^{miss} intervals (right) for the targeted analysis, including the b-veto. Based on this we chose $K = 0.13 \pm 0.02$ for the E_T^{miss} regions up to $E_T^{miss} > 100$ GeV. For higher E_T^{miss} regions we chose $K = 0.13 \pm 0.07$.

6.3 Estimating the WZ and ZZ Background with MC

Backgrounds from $W(\ell\nu)Z(\ell\ell)$ where the W lepton is not identified or is outside acceptance, and $Z(\nu\nu)Z(\ell\ell)$, are estimated from simulation. The MC modeling of these processes is validated by comparing the MC predictions with data in control samples with exactly 3 leptons (WZ control sample) and exactly 4 leptons (ZZ control sample). The critical samples are the WZJetsTo3LNu and ZZJetsTo4L, listed in Table 1 (the WZJetsTo2L2Q, ZZJetsTo2L2Q, and ZZJetsTo2L2Nu samples are also used in this analysis but their contribution to the 3-lepton and 4-lepton control samples is negligible).

6.3.1 WZ Validation Studies

A pure WZ sample can be selected in data with the requirements:

- Exactly 3 $p_T > 20$ GeV leptons passing analysis identication and isolation requirements,

- 2 of the 3 leptons must fall in the Z window 81-101 GeV,

- $E_T^{miss} > 50$ GeV (to suppress DY).

The data and MC yields passing the above selection are in Table 7. The inclusive yields (without any jet requirements) agree within 13%, which is consistent within the uncertainty in the CMS measured WZ cross section (17%). A data vs. MC comparison of kinematic distributions (jet multiplicity, E_T^{miss}, Z p_T) is given in Fig. 8. High E_T^{miss} values in WZ and ZZ events arise from highly boosted W or Z bosons that decay leptonically, and we therefore check that the MC does a reasonable job of reproducing the p_T distributions of the leptonically decaying Z . While the inclusive WZ yields are in reasonable agreement, we observe an excess in data in events with at least 2 jets, corresponding to the jet multiplicity requirement in our preselection. We observe 106 events in data while the MC predicts 62 ± 1.5 (stat), representing an excess of 71%, as indicated in Table 8. This excess will be studied further. For the time being, based on these studies we currently assess an uncertainty of 70% on the WZ yield.

Table 7: Data and Monte Carlo yields passing the WZ preselection.

Sample	ee	$\mu\mu$	eμ	total
WZ	116.7 ± 0.8	151.5 ± 0.8	8.1 ± 0.2	276.3 ± 1.2
ttV	4.1 ± 0.2	4.9 ± 0.2	1.2 ± 0.1	10.2 ± 0.3
$t\bar{t}$	1.2 ± 0.6	3.2 ± 0.9	3.6 ± 1.0	7.9 ± 1.5
ZZ	2.5 ± 0.0	3.4 ± 0.0	0.2 ± 0.0	6.1 ± 0.0
$Z + \text{jets}$	1.2 ± 0.9	3.0 ± 1.8	0.0 ± 0.0	4.2 ± 2.1
vvv	1.6 ± 0.1	2.1 ± 0.1	0.3 ± 0.0	4.0 ± 0.1
single top	0.0 ± 0.0	0.2 ± 0.2	0.0 ± 0.0	0.2 ± 0.2
WW	0.0 ± 0.0	0.0 ± 0.0	0.1 ± 0.0	0.1 ± 0.1
tot SM MC	127.3 ± 1.4	168.4 ± 2.3	13.5 ± 1.0	309.2 ± 2.8
data	156	178	16	350

Table 8: Data and Monte Carlo yields passing the WZ preselection and $N_{\text{jets}} > 2$.

Sample	ee	$\mu\mu$	eμ	total
WZ	19.1 ± 0.3	24.6 ± 0.3	1.3 ± 0.1	44.9 ± 0.5
ttV	3.8 ± 0.2	4.5 ± 0.2	1.0 ± 0.1	9.3 ± 0.3
$t\bar{t}$	0.8 ± 0.5	1.6 ± 0.7	0.9 ± 0.5	3.3 ± 1.0
ZZ	0.5 ± 0.0	0.7 ± 0.0	0.0 ± 0.0	1.2 ± 0.0
$Z + \text{jets}$	0.9 ± 0.9	0.0 ± 0.0	0.0 ± 0.0	0.9 ± 0.9
vvv	0.9 ± 0.0	1.2 ± 0.1	0.1 ± 0.0	2.2 ± 0.1
single top	0.0 ± 0.0	0.2 ± 0.2	0.0 ± 0.0	0.2 ± 0.2
WW	0.0 ± 0.0	0.0 ± 0.0	0.0 ± 0.0	0.0 ± 0.0
tot SM MC	25.9 ± 1.1	32.9 ± 0.8	3.3 ± 0.5	62.1 ± 1.5
data	47	51	8	106

13
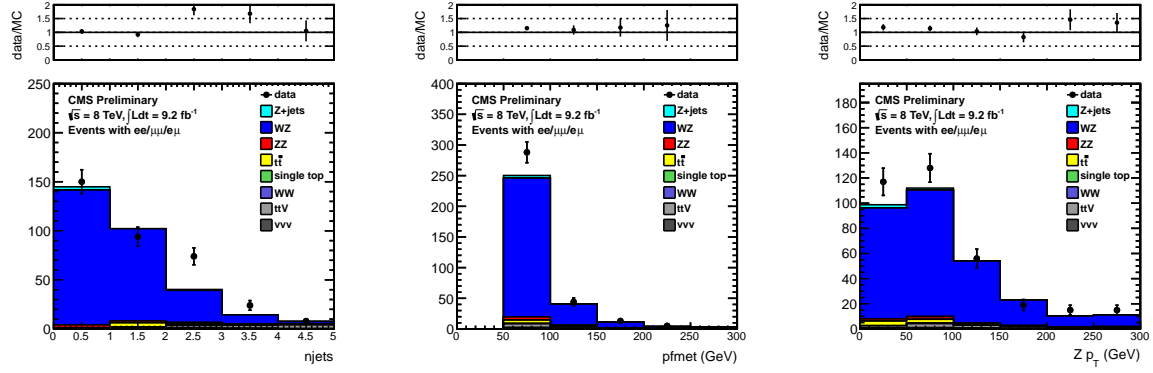
Figure 8: Data vs. MC comparisons for the WZ selection discussed in the text for 9.2 fb^{-1}. The number of jets, missing transverse energy, and Z boson transverse momentum are displayed.

6.3.2   ZZ Validation Studies

A pure ZZ sample can be selected in data with the requirements:

• Exactly 4 $p_T > 20$ GeV leptons passing analysis identication and isolation requirements,

• 2 of the 4 leptons must fall in the Z window 81-101 GeV.

The data and MC yields passing the above selection are in Table 9. In this ZZ-dominated sample we observe good
agreement between the data yield and the MC prediction. After requiring 2 jets (corresponding to the requirement
in the analysis selection), we observe 4 events in data and the MC predicts 6.6 ± 0.1 events. Due to the limited
statistical precision we assign an uncertainty fo 50% on the ZZ yield.

Table 9: Data and Monte Carlo yields for the ZZ preselection.

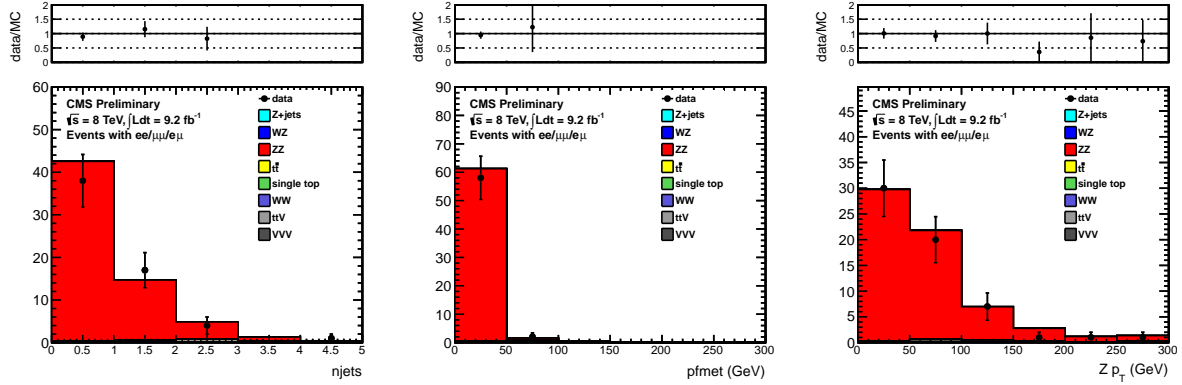| Sample	ee	$\mu\mu$	eμ	total
ZZ	25.1 ± 0.1	34.9 ± 0.1	1.6 ± 0.0	61.7 ± 0.1
ttV	0.6 ± 0.1	0.6 ± 0.1	0.2 ± 0.0	1.4 ± 0.1
VVV	0.3 ± 0.0	0.4 ± 0.0	0.0 ± 0.0	0.7 ± 0.0
WZ	0.1 ± 0.0	0.1 ± 0.0	0.0 ± 0.0	0.1 ± 0.0
$Z +$ jets	0.0 ± 0.0	0.0 ± 0.0	0.0 ± 0.0	0.0 ± 0.0
$t\bar{t}$	0.0 ± 0.0	0.0 ± 0.0	0.0 ± 0.0	0.0 ± 0.0
single top	0.0 ± 0.0	0.0 ± 0.0	0.0 ± 0.0	0.0 ± 0.0
WW	0.0 ± 0.0	0.0 ± 0.0	0.0 ± 0.0	0.0 ± 0.0
tot SM MC	26.1 ± 0.1	36.1 ± 0.1	1.8 ± 0.0	63.9 ± 0.2
data	24	36	0	60

Figure 9: Data vs. MC comparisons for the ZZ selection discussed in the text for 9.2 fb^{-1}. The number of jets, missing transverse energy, and Z boson transverse momentum are displayed.

15

7 Results

In this section we provide the results of the inclusive and targeted searches. The observed and predicted E_T^{miss} distributions for the inclusive analysis are indicated in Fig. 10. A summary of the results in the signal regions is provided in Table 10. Currently we blind the observed data yields for the signal regions, defined by $E_T^{miss} > 100$ GeV. These yields will be presented when the decision is made to unblind the Z region for the Aachen/ETH low-mass opposite-sign same-flavor dilepton analysis ("edge analysis"). In the low E_T^{miss} region, we observe good agreement between the data and the predicted background, which validates the background estimation methodology. The separate results for the ee and $\mu\mu$ channels are presented in App. B.
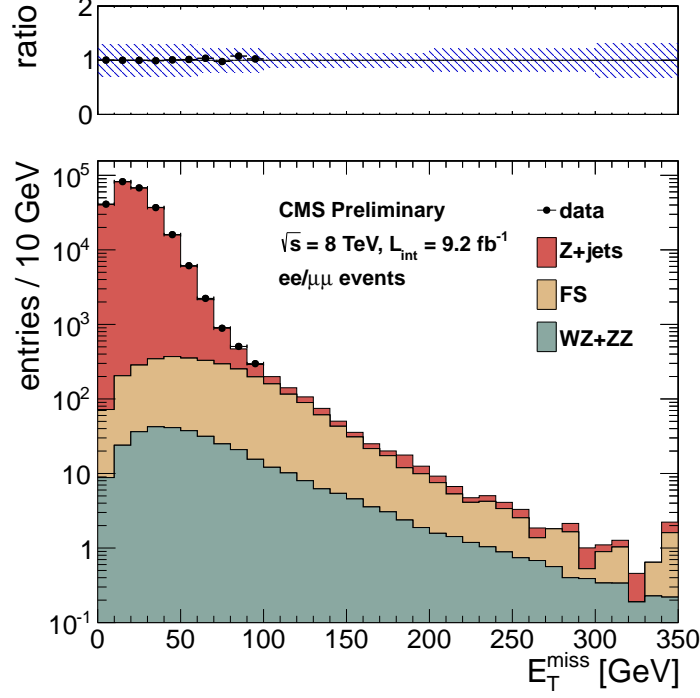

Figure 10: Results of the inclusive analysis. The observed E_T^{miss} distribution (black points) is compared with the sum of the predicted E_T^{miss} distributions from $Z + \mathrm{jets}$, flavor-symmetric backgrounds, and WZ+ZZ backgrounds. The ratio of observed to predicted yields in each bin is indicated. The error bars indicate the statistical uncertainty in the data and the shaded band indicates the total background uncertainty.

Table 10: Summary of results in the inclusive analysis. The total background is the sum of the $Z + \mathrm{jets}$ background predicted from the E_T^{miss} templates method ($Z + \mathrm{jets}$ bkg), the flavor-symmetric background predicted from eμ events (FS bkg), and the WZ and ZZ backgrounds predicted from MC (WZ bkg and ZZ bkg). All uncertainties include both the statistical and systematic components. The Gaussian significance of the deviation between the data and total background is indicated for signal regions with at least 20 observed events.

	E_T^{miss} 0–30 GeV	E_T^{miss} 30–60 GeV	E_T^{miss} 60–100 GeV	E_T^{miss} 100–200 GeV	E_T^{miss} 200–300 GeV	E_T^{miss} > 300 GeV
$Z + \mathrm{jets}$ bkg	190124 ± 57038	57993 ± 17399	2744 ± 824	123 ± 37	7.4 ± 2.4	1.3 ± 0.5
FS bkg	492 ± 77	947 ± 147	981 ± 152	503 ± 78	23.6 ± 7.1	3.0 ± 1.9
WZ bkg	61.5 ± 43.0	104.8 ± 73.4	75.4 ± 52.8	41.2 ± 28.8	5.6 ± 3.9	1.6 ± 1.6
ZZ bkg	7.6 ± 3.8	16.2 ± 8.1	17.4 ± 8.7	16.1 ± 8.1	3.2 ± 1.6	1.0 ± 1.0
total bkg	190685 ± 57038	59061 ± 17400	3818 ± 840	683 ± 92	39.9 ± 8.6	6.9 ± 2.7
data	190793	58953	3921	?	?	?
significance	0.0	-0.0	0.1	?	?	?

The observed and predicted E_T^{miss} distributions for the targeted analysis are indicated in Fig. 11. A summary of
the results in the signal regions is provided in Table 11. Here the results in the signal regions with $E_T^{miss} > 100$
GeV region are also blinded, pending completion of signal optimization studies (see Sec. 8). The observed yields
are in good agreement with the predicted background the low E_T^{miss} region, validating the background estimation
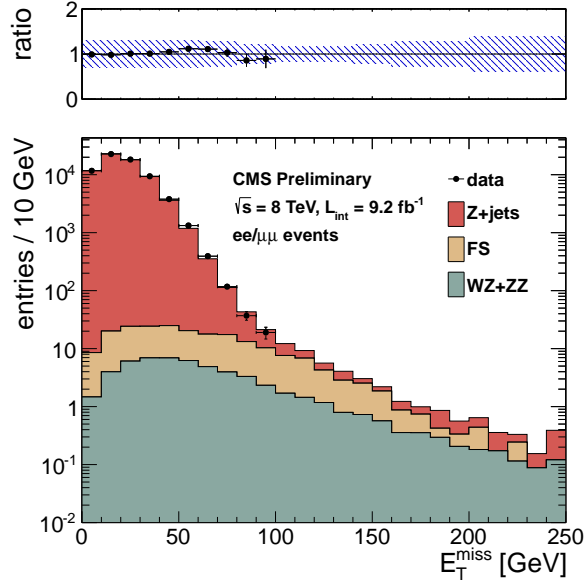methodology.

Figure 11: Results of the targeted analysis. The observed E_T^{miss} distribution (black points) is compared with the
sum of the predicted E_T^{miss} distributions from Z + jets , flavor-symmetric backgrounds, and WZ+ZZ backgrounds.
The ratio of observed to predicted yields in each bin is indicated. The error bars indicate the statistical uncertainty
in the data and the shaded band indicates the total background uncertainty.

Table 11: Summary of results in the targeted analysis. The total background is the sum of the Z + jets background
predicted from the E_T^{miss} templates method (Z + jets bkg), the flavor-symmetric background predicted from eμ
events (FS bkg), and the WZ and ZZ backgrounds predicted from MC (WZ bkg and ZZ bkg). All uncertainties
include both the statistical and systematic components. The Gaussian significance of the deviation between the
data and total background is indicated for signal regions with at least 20 observed events.

	E_T^{miss} 0–30 GeV	E_T^{miss} 30–60 GeV	E_T^{miss} 60–80 GeV	E_T^{miss} 80–100 GeV	E_T^{miss} 100–120 GeV
Z + jets bkg	52823 ± 15847	14015 ± 4205	433 ± 130	40.9 ± 12.4	7.0 ± 2.2
FS bkg	41.3 ± 7.2	49.5 ± 8.6	26.4 ± 4.7	17.9 ± 3.3	11.3 ± 2.2
WZ bkg	9.5 ± 6.6	15.9 ± 11.2	6.6 ± 4.7	3.9 ± 2.7	2.1 ± 1.5
ZZ bkg	2.1 ± 1.0	4.1 ± 2.1	2.2 ± 1.1	1.8 ± 0.9	1.0 ± 0.5
total bkg	52876 ± 15847	14085 ± 4205	468 ± 130	64.4 ± 13.2	21.5 ± 3.5
data	52485	14476	510	56	?
significance	-0.0	0.1	0.3	-0.6	?
	E_T^{miss} 120–140 GeV	E_T^{miss} 140–160 GeV	E_T^{miss} 160–180 GeV	E_T^{miss} 180–200 GeV	E_T^{miss} > 200 GeV
Z + jets bkg	2.6 ± 0.8	0.9 ± 0.3	0.6 ± 0.2	0.7 ± 0.3	0.8 ± 0.3
FS bkg	5.1 ± 1.2	3.1 ± 0.8	0.9 ± 0.5	0.3 ± 0.2	0.4 ± 0.3
WZ bkg	1.1 ± 0.8	0.8 ± 0.6	0.4 ± 0.3	0.3 ± 0.2	0.5 ± 0.5
ZZ bkg	0.8 ± 0.4	0.5 ± 0.3	0.4 ± 0.2	0.2 ± 0.1	0.7 ± 0.7
total bkg	9.7 ± 1.7	5.2 ± 1.1	2.2 ± 0.6	1.4 ± 0.4	2.3 ± 0.9
data	?	?	?	?	?
significance	?	?	?	?	?

8 Signal Optimization Studies

In this section we describe ongoing work to optimize the targeted analysis for the $WZ + E_T^{miss}$ signal scenario (see Fig. 1 right). Here we optimize the expected cross section upper limits using the predicted backgrounds in the signal regions. The observed yields for the $E_T^{miss} > 100$ GeV signal regions will be unblinded after these studies are completed.

We are currently exploring several handles to optimize the signal sensitivity:

- b-tagging. For the current results, we veto events containing a b-jet identified using the CSV medium working point. Since the background prior to the b-jet veto is dominated by $t\bar{t}$, the size of the expected background passing the final selection depends strongly on the choice of this working point. For example, switching to the loose working point reduces the expected background in the $E_T^{miss} > 100$ GeV region by nearly a factor of 2, as shown in Table 12, which should be compared with Table 11. However this reduces the signal efficiency by $\sim$20–25%.

- Z mass requirement. The $t\bar{t}$ background is roughly flat vs. dilepton mass; hence the $t\bar{t}$ background is approximately proportional to the size of the Z mass window. Thus the signal-to-background ratio can in principle be improved by tightening the Z mass requirement.

- dijet mass requirement. For all backgrounds, the dijet mass distribution is smooth and broad, as shown in Fig. 5. However the signal dijet mass distribution is more strongly peaked near the W/Z boson mass.

- E_T^{miss} reconstruction. The E_T^{miss} resolution in 8 TeV data is significantly degraded with respect to 7 TeV data due to the large pile-up. As a result, the $Z + \text{jets}$ background satisfying moderate E_T^{miss} requirements of $\sim$80–100 GeV is significantly enhanced. This is the E_T^{miss} region with the maximum sensitivity to low mass ($\sim$150 GeV) charginos and neutralinos. Hence the sensitivity of the analysis may be improved by using a flavor of E_T^{miss} reconstruction which is more robust to pile-up effects. An example, which is used in the Higgs$\rightarrow$WW analysis, is called "track-E_T^{miss};" this is simply the E_T^{miss} reconstructed from charged particles with a dz requirement which ensures that the particles originate from the signal primary vertex.

The optimization of the requirements to maximize the sensitivity of the analysis is ongoing.

Table 12: Summary of results in the targeted analysis with the loose working point of the CSV tagger used for the b-jet veto. The total background is the sum of the $Z + \text{jets}$ background predicted from the E_T^{miss} templates method ($Z + \text{jets}$ bkg), the flavor-symmetric background predicted from eμ events (FS bkg), and the WZ and ZZ backgrounds predicted from MC (WZ bkg and ZZ bkg). All uncertainties include both the statistical and systematic components. The Gaussian significance of the deviation between the data and total background is indicated for signal regions with at least 20 observed events.

	E_T^{miss} 0–30 GeV	E_T^{miss} 30–60 GeV	E_T^{miss} 60–80 GeV	E_T^{miss} 80–100 GeV	E_T^{miss} 100–120 GeV
$Z + \text{jets}$ bkg	38839 ± 11652	10441 ± 3133	322 ± 97	29.7 ± 9.1	3.8 ± 1.2
FS bkg	23.9 ± 4.3	23.9 ± 4.3	12.2 ± 2.4	6.3 ± 1.4	5.0 ± 1.2
WZ bkg	6.3 ± 4.4	10.4 ± 7.3	4.4 ± 3.1	2.6 ± 1.8	1.5 ± 1.0
ZZ bkg	1.6 ± 0.8	3.1 ± 1.6	1.7 ± 0.9	1.4 ± 0.7	0.8 ± 0.4
total bkg	38871 ± 11652	10479 ± 3133	340 ± 97	39.9 ± 9.4	11.1 ± 2.0
data	38545	10805	381	40	?
significance	-0.0	0.1	0.4	0.0	?

	E_T^{miss} 120–140 GeV	E_T^{miss} 140–160 GeV	E_T^{miss} 160–180 GeV	E_T^{miss} 180–200 GeV	E_T^{miss} > 200 GeV
$Z + \text{jets}$ bkg	1.8 ± 0.6	0.7 ± 0.2	0.5 ± 0.2	0.6 ± 0.2	0.5 ± 0.2
FS bkg	2.1 ± 0.6	1.3 ± 0.5	0.6 ± 0.4	0.1 ± 0.1	0.1 ± 0.1
WZ bkg	0.7 ± 0.5	0.5 ± 0.4	0.2 ± 0.2	0.2 ± 0.2	0.3 ± 0.3
ZZ bkg	0.6 ± 0.3	0.4 ± 0.2	0.3 ± 0.1	0.2 ± 0.1	0.5 ± 0.5
total bkg	5.1 ± 1.0	2.9 ± 0.7	1.7 ± 0.5	1.1 ± 0.3	1.4 ± 0.6
data	?	?	?	?	?
significance	?	?	?	?	?

9 Interpretation

The results of this search will be interpreted in the context of simplified model spectra (SMS). For the inclusive analysis, we will use the T5zz model depicted in Fig. 1 (left). For the targeted analysis, we will use the $WZ + E_T^{miss}$ model depicted in Fig. 1 (right), and a GMSB model which produces a signature of $ZZ + E_T^{miss}$. For the $WZ + E_T^{miss}$

model (GMSB ZZ + E_T^{miss} model), the results of this analysis will be combined with the results of searches for charginos and neutralinos in the trilepton (quadlepton) final state.

10 Summary

This note presents a search for BSM physics in final states with leptonically-decaying Z bosons, jets, and E_T^{miss}. Two strategies were pursued. The first is an inclusive approach which targets BSM scenarios with Z bosons produced in the decays of strongly-interacting particles. The second is a targeted approach which focuses on BSM scenarios where the Z bosons are produced in the decays of weakly-interacting particles. The main backgrounds are estimated with data-driven techniques. Good agreement is observed between the data and the predicted backgrounds in the control regions defined by $E_T^{miss} < 100$ GeV. The data yields in the signal region of the inclusive analysis will be presented when the decision to unblind the Z region of the edge analysis is taken. The data yields of the targeted analysis will be presented after completion of signal optimization studies.

References

[1] CMS Collaboration, "Search for physics beyond the standard model in events with a Z boson, jets, and missing transverse energy in pp collisions at $\sqrt{s} = 7$ TeV,", arXiv:1204.3774v1 [hep-ex].

[2] SUS-12-006, paper draft

[3] https://twiki.cern.ch/twiki/bin/viewauth/CMS/EgammaCutBasedIdentification

[4] https://twiki.cern.ch/twiki/bin/viewauth/CMS/EgammaEARhoCorrection

[5] https://twiki.cern.ch/twiki/bin/view/CMSPublic/SWGuideMuonId

[6] M. Chen, AN 2012/237 "Interpretation of the Same-Sign di-leptons with bjets and MET search"

A   Z Background Predictions for the "Edge Analysis"

The Aachen and ETH groups have reported an excess of low-mass, opposite-sign same-flavor events (see AN 2012/200 and AN 2012/231). In this section we derive predictions for the Z background in the Z mass regions for the two signal regions used for this analysis. We then use this prediction to derive an estimate of the low-mass γ^*/Z contribution using an extrapolation technique commonly referred to as the "$R_{out/in}$" technique. All results in this section are for 5.1 fb^{-1} only and will be updated to the full data sample after the Z region of the edge analysis is unblinded. The two signal regions are defined as:

- Low-E_T^{miss} signal region (ETH)
    - 2 $p_T > 20$ GeV leptons with $|\eta| < 2.4$
    - At least 3 jets ($p_T > 40$ GeV, $|\eta| < 3$)
    - $E_T^{miss} > 100$ GeV
- High-E_T^{miss} signal region (Aachen)
    - leading lepton $p_T > 20$ GeV, trailing lepton $p_T > 10$ GeV, both with $|\eta| < 2.4$
    - At least 2 jets ($p_T > 40$ GeV, $|\eta| < 3$) with scalar sum $H_T > 100$ GeV
    - $E_T^{miss} > 150$ GeV

We begin with a synchronization exercise to make sure that we can reproduce the ETH/Aachen results. In Table 13 we display the yields in the Z mass regions of the 2 signal regions and compare these to results from the ETH and Aachen groups. In general we observe agreement at the level of a few % and are working to iron out the remaining differences.

Table 13: Summary of the synchronization exercise with the ETH and Aachen groups. The yields in the Z mass region are displayed for the low E_T^{miss} and high E_T^{miss} signal regions.

low E_T^{miss} signal region	UCSB-UCSD-FNAL	ETH
ee	115	117
$\mu\mu$	168	171
eμ	207	214

high E_T^{miss} signal region	UCSB-UCSD-FNAL	Aachen
ee	83	84
$\mu\mu$	99	105
eμ	134	134

In order to adapt the E_T^{miss} templates method to predict the Z background in these regions, we make the following modifications to the background estimation methodology. First, the FS background scaling factor K must be modified for the High-E_T^{miss} signal region since relaxing the trailing lepton p_T requirement to 10 GeV changes the shape of the dilepton mass distribution. The results are shown in Fig. 12. Based on this plot we choose $K = 0.13 \pm 0.02$ for E_T^{miss} signal regions up to 200 GeV; for E_T^{miss} 200-300 GeV and $E_T^{miss} > 300$ GeV we inflate the uncertainty to $K = 0.13 \pm 0.04$ and $K = 0.13 \pm 0.05$, respectively, due to the limited statistical precision. We also check the K scaling factor after requiring 3 high p_T jets as used for the Low-E_T^{miss} signal region, as displayed in Fig. 13. Based on this plot we choose $K = 0.14 \pm 0.02$ for E_T^{miss} signal regions up to 200 GeV; for E_T^{miss} 200-300 GeV and $E_T^{miss} > 300$ GeV we inflate the uncertainty to $K = 0.14 \pm 0.03$ and $K = 0.14 \pm 0.07$, respectively. In addition, we change the jet p_T threshold for the E_T^{miss} templates jet multiplicity binning from 30 to 40 GeV, and change the H_T bins to (0,80,100,150,200,250,300,5000) GeV.

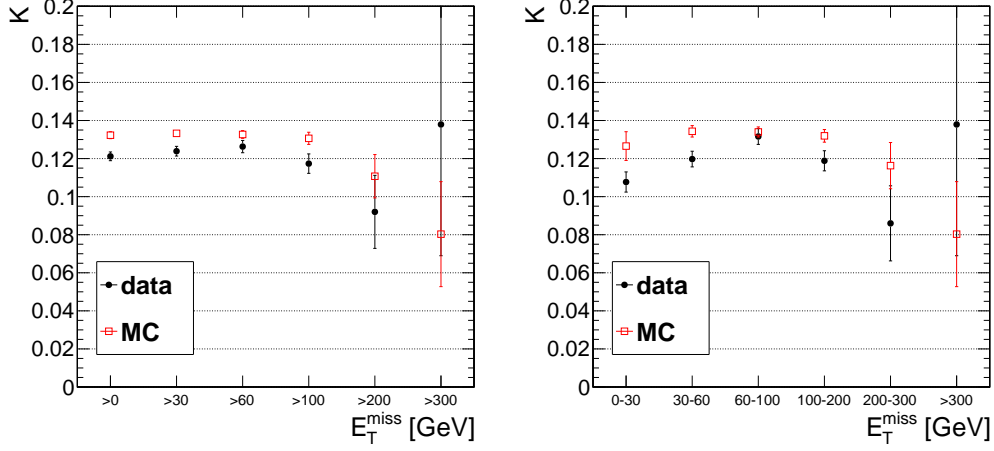Figure 12: The efficiency for eμ events to satisfy the dilepton mass requirement, K, in data and simulation for inclusive E_T^{miss} intervals (left) and exclusive E_T^{miss} intervals (right) for the dilepton $p_T > (20,10)$ GeV selection with at least 2 $p_T > 40$ GeV jets (used for the high E_T^{miss} signal region).
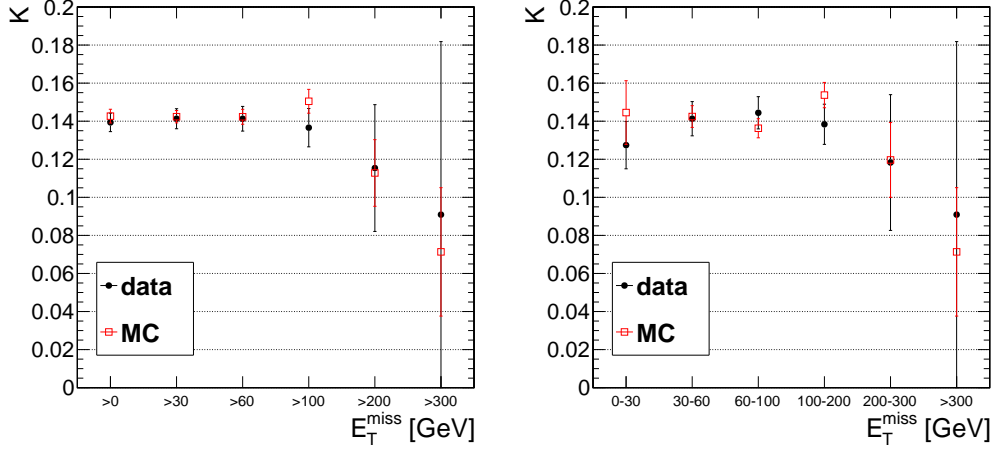

Figure 13: The efficiency for eμ events to satisfy the dilepton mass requirement, K, in data and simulation for inclusive E_T^{miss} intervals (left) and exclusive E_T^{miss} intervals (right) for the dilepton $p_T > (20,20)$ GeV selection with at least 3 $p_T > 40$ GeV jets (used for the low E_T^{miss} signal region).

The strategy is to select Z$\to \ell\ell$ candidates ($81 < m_{\ell\ell} < 101$ GeV) and the jet requirements corresponding to the low-E_T^{miss} and high-E_T^{miss} signal regions, and compare the observed E_T^{miss} distribution to the sum of the predictions from the $Z + jets$ background (from the E_T^{miss} templates method based on the $\gamma + jets$ data control sample), the flavor-symmetric background predicted from eμ data events, and MC contributions from WZ/ZZ, as well as the rare SM processes with Z bosons ($t\bar{t}Z$ and ZZZ, ZZW, ZWW). The results of the low E_T^{miss} signal region are displayed in Fig. 14 and summarized in Table 14. Good agreement is observed in the low E_T^{miss} region ($E_T^{miss} <$ 100 GeV), as well as in the high E_T^{miss} tail region ($E_T^{miss} > 200$ GeV). We observe a slight excess in the moderate E_T^{miss} region (E_T^{miss} 100–200 GeV), which is split approximately evenly between the ee and $\mu\mu$ channels. For the requirement $E_T^{miss} > 100$ GeV corresponding to the low E_T^{miss} signal region, we observe 175 events and predict a total background of 138 ± 18 events, corresponding to an excess of 1.6σ. The results of the high E_T^{miss} signal region are displayed in Fig. 15 and summarized in Table 15. Good agreement is observed across the full E_T^{miss} region. For the requirement $E_T^{miss} > 150$ GeV corresponding to the high E_T^{miss} signal region, we observe 95 events and predict a total background of 98 ± 14 events.
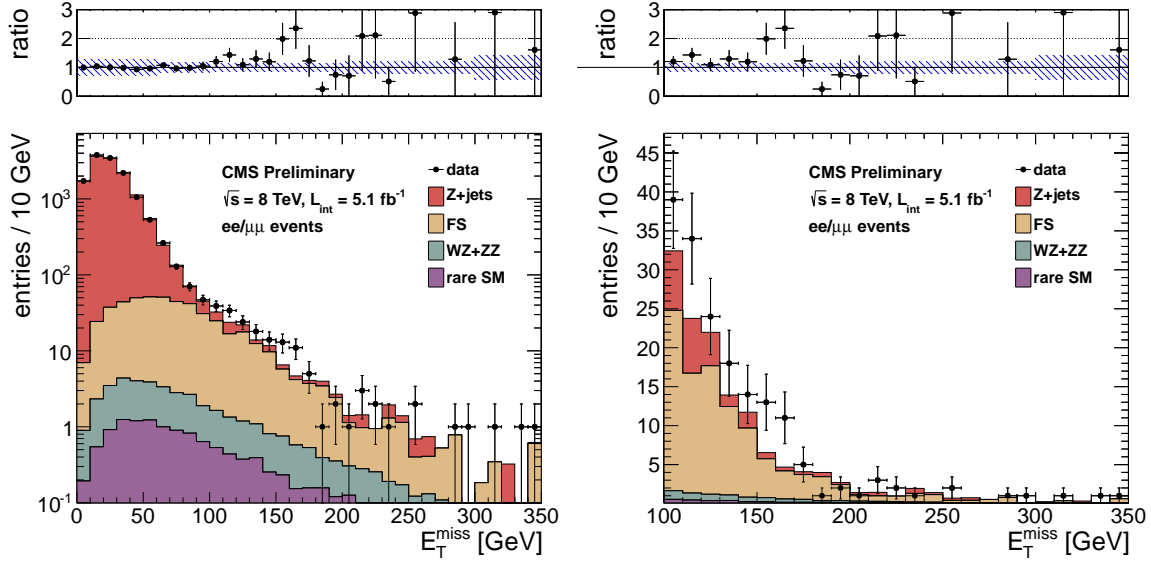
22

Figure 14: Results of the inclusive analysis for the low E_T^{miss} signal region. The left plot shows the full E_T^{miss} range, the right plot is zoomed in on the $E_T^{miss} > 100$ GeV region. The observed E_T^{miss} distribution (black points) is compared with the sum of the predicted E_T^{miss} distributions from $Z + \text{jets}$, flavor-symmetric backgrounds, WZ+ZZ backgrounds, and rare SM backgrounds. The ratio of observed to predicted yields in each bin is indicated. The error bars indicate the statistical uncertainty in the data and the shaded band indicates the total background uncertainty.

Table 14: Summary of results in the inclusive analysis for the low E_T^{miss} signal region. The total background is the sum of the $Z + \text{jets}$ background predicted from the E_T^{miss} templates method ($Z + \text{jets}$ bkg), the flavor-symmetric background predicted from $e\mu$ events (FS bkg), the WZ and ZZ backgrounds predicted from MC (WZ bkg and ZZ bkg) and the rare SM backgrounds. All uncertainties include both the statistical and systematic components. The Gaussian significance of the deviation between the data and total background is indicated for signal regions with at least 20 observed events.

|	$E_T^{miss} > 0$ GeV	$E_T^{miss} > 30$ GeV	$E_T^{miss} > 60$ GeV	$E_T^{miss} > 100$ GeV	$E_T^{miss} > 200$ GeV	$E_T^{miss} > 300$ GeV
$Z + \text{jets}$ bkg	12870 ± 3862	4118 ± 1236	356 ± 107	27.5 ± 8.5	2.6 ± 1.1	0.3 ± 0.3
FS bkg	451 ± 70	389 ± 61	256 ± 40	99.1 ± 15.8	6.9 ± 1.8	1.0 ± 0.6
WZ bkg	24.1 ± 16.9	19.5 ± 13.7	11.8 ± 8.3	5.6 ± 3.9	1.1 ± 1.0	0.2 ± 0.2
ZZ bkg	4.3 ± 2.2	3.9 ± 2.0	3.0 ± 1.5	1.9 ± 1.0	0.5 ± 0.4	0.1 ± 0.1
rare SM bkg	12.2 ± 6.1	10.5 ± 5.3	6.9 ± 3.5	3.5 ± 1.8	0.7 ± 0.6	0.2 ± 0.2
total bkg	13362 ± 3862	4541 ± 1238	634 ± 115	138 ± 18	11.8 ± 2.5	1.8 ± 0.8
data	13412	4461	684	175	14	3
significance	0.0	-0.1	0.4	1.6	0.5	
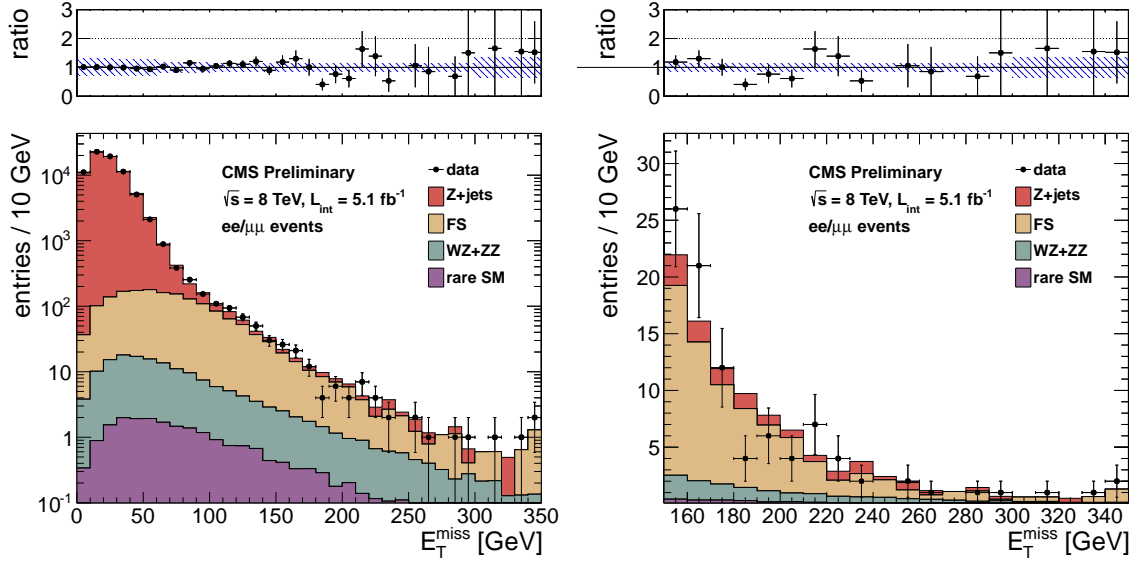
Figure 15: Results of the inclusive analysis for the high E_T^{miss} signal region. The left plot shows the full E_T^{miss} range, the right plot is zoomed in on the $E_T^{miss} > 100$ GeV region. The observed E_T^{miss} distribution (black points) is compared with the sum of the predicted E_T^{miss} distributions from $Z + \text{jets}$, flavor-symmetric backgrounds, WZ+ZZ backgrounds, and rare SM backgrounds. The ratio of observed to predicted yields in each bin is indicated. The error bars indicate the statistical uncertainty in the data and the shaded band indicates the total background uncertainty.

Table 15: Summary of results in the inclusive analysis for the high E_T^{miss} signal region. The total background is the sum of the $Z + \text{jets}$ background predicted from the E_T^{miss} templates method ($Z + \text{jets}$ bkg), the flavor-symmetric background predicted from eμ events (FS bkg), the WZ and ZZ backgrounds predicted from MC (WZ bkg and ZZ bkg) and the rare SM backgrounds. All uncertainties include both the statistical and systematic components. The Gaussian significance of the deviation between the data and total background is indicated for signal regions with at least 20 observed events.

|	$E_T^{miss} > 0$ GeV	$E_T^{miss} > 30$ GeV	$E_T^{miss} > 60$ GeV	$E_T^{miss} > 100$ GeV	$E_T^{miss} > 150$ GeV	$E_T^{miss} > 300$ GeV
$Z + \text{jets}$ bkg	71975 ± 21593	19573 ± 5873	1182 ± 355	70.7 ± 21.4	13.6 ± 4.2	0.4 ± 0.4
FS bkg	1540 ± 255	1293 ± 214	823 ± 136	313 ± 52	68.6 ± 11.7	2.4 ± 1.1
WZ bkg	115.9 ± 81.2	91.8 ± 64.3	52.1 ± 36.5	22.4 ± 15.7	8.9 ± 6.3	0.8 ± 0.8
ZZ bkg	22.6 ± 11.3	20.3 ± 10.2	15.1 ± 7.6	8.8 ± 4.5	4.3 ± 2.3	0.5 ± 0.5
rare SM bkg	20.6 ± 10.3	17.9 ± 9.0	12.0 ± 6.1	6.3 ± 3.2	2.8 ± 1.5	0.3 ± 0.3
total bkg	73674 ± 21595	20996 ± 5877	2084 ± 382	421 ± 59	98.1 ± 14.2	4.5 ± 1.5
data	73711	20601	2121	446	95	4
significance	0.0	-0.1	0.1	0.4	-0.2	
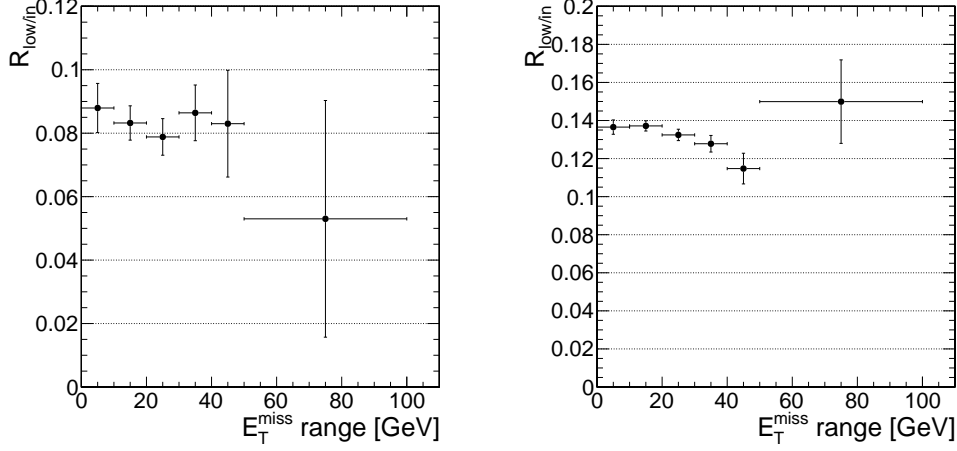
Figure 16: The ratio $R_{low/in}$ of low mass ($15 < m_{\ell\ell} < 70$ GeV) to on-Z ($81 < m_{\ell\ell} < 101$ GeV) events, as a function of the E_T^{miss} requirement. The left plot corresponds to the low E_T^{miss} signal region (2 $p_T > 20$ GeV leptons with at least 3 jets), the right plot corresponds to the high E_T^{miss} signal region ($p_T > (20,10)$ GeV leptons with at least 2 jets).

Given a prediction for the Z background in the Z mass window, we can extrapolate to estimate the low mass γ^*/Z contribution. We extract the ratio $R_{low/in}$ of low-mass to on-shell Z events from data, correcting for the contribution from flavor-symmetric backgrounds, according to:

$$R_{low/in} = (N_{SF}^{low} - N_{OF}^{low})/(N_{SF}^{in} - N_{OF}^{in}). \tag{2}$$

Here SF and OF refer to the same-flavor and opposite-flavor data yields in the "low" ($15 < m_{\ell\ell} < 70$ GeV) and "in" ($81 < m_{\ell\ell} < 101$ GeV) dilepton mass regions. To predict the low-mass γ^*/Z contribution, we scale the total predicted Z background by this quantity, which is displayed in Fig. 16. Here we measure $R_{low/in}$ in several E_T^{miss} regions, and assess the uncertainty based on the variation with respect to E_T^{miss}. Based on this plot we choose $R_{low/in} = 0.08 \pm 0.02$ for the low E_T^{miss} signal region and $R_{low/in} = 0.13 \pm 0.03$ for the high E_T^{miss} region. For the low E_T^{miss} signal region, the total predicted Z background in the Z mass region is 39 ± 9.6 (sum of the Z + jets WZ+ZZ, and rare SM backgrounds from Table 14 $E_T^{miss} > 100$ GeV), resulting in a γ^*/Z prediction of 3.1 ± 1.1 events. For the high E_T^{miss} signal region, the total predicted Z background in the Z mass region is 30 ± 8.1 (sum of the Z + jets WZ+ZZ, and rare SM backgrounds from Table 14 $E_T^{miss} > 150$ GeV), resulting in a γ^*/Z prediction of 3.8 ± 1.4 events.

Hence we summarize the results as:

- Low E_T^{miss} signal region
    - Total predicted background in Z mass region: 138 ± 18 events
    - Total observed yield in Z mass region: 175 events ($+1.6\sigma$)
    - Low-mass $\gamma*$/Z prediction: 3.1 ± 1.1 events

- High E_T^{miss} signal region
    - Total predicted background in Z mass region: 98 ± 14 events
    - Total observed yield in Z mass region: 95 events (-0.2σ)
    - Low-mass $\gamma*$/Z prediction: 3.8 ± 1.4 events

B Results in the ee and $\mu\mu$ Channels

In this section we provide the results of the inclusive and targeted searches, separately in the ee and $\mu\mu$ channels. The E_T^{miss} distributions in the inclusive analysis for the ee channel are displayed in Fig. 17 and the signal region yields are presented in Table 16. The E_T^{miss} distributions in the inclusive analysis for the $\mu\mu$ channel are displayed in Fig. 18 and the signal region yields are presented in Table 17.
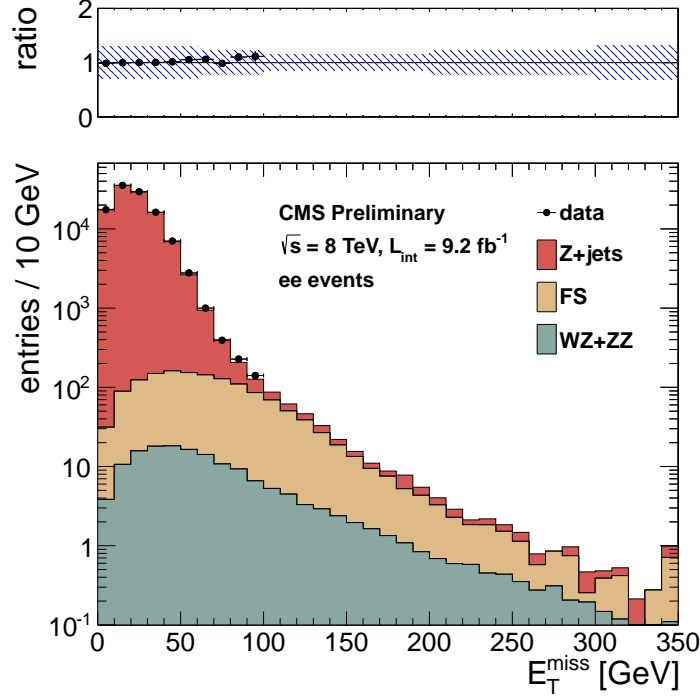

Figure 17: Results of the inclusive analysis in the ee channel. The observed E_T^{miss} distribution (black points) is compared with the sum of the predicted E_T^{miss} distributions from $Z + \text{jets}$, flavor-symmetric backgrounds, and WZ+ZZ backgrounds. The ratio of observed to predicted yields in each bin is indicated. The error bars indicate the statistical uncertainty in the data and the shaded band indicates the total background uncertainty.

Table 16: Summary of results in the inclusive analysis in the ee channel. The total background is the sum of the $Z+\text{jets}$ background predicted from the E_T^{miss} templates method ($Z+\text{jets}$ bkg), the flavor-symmetric background predicted from eμ events (FS bkg), and the WZ and ZZ backgrounds predicted from MC (WZ bkg and ZZ bkg). All uncertainties include both the statistical and systematic components. The Gaussian significance of the deviation between the data and total background is indicated for signal regions with at least 20 observed events.

|	E_T^{miss} 0–30 GeV	E_T^{miss} 30–60 GeV	E_T^{miss} 60–100 GeV	E_T^{miss} 100–200 GeV	E_T^{miss} 200–300 GeV	E_T^{miss} > 300 GeV
$Z + \text{jets}$ bkg	82301 ± 24696	25208 ± 7570	1204 ± 371	54.8 ± 40.1	3.3 ± 1.1	0.6 ± 0.2
FS bkg	214 ± 40	411 ± 77	426 ± 80	218 ± 41	10.2 ± 3.3	1.3 ± 0.8
WZ bkg	26.9 ± 18.9	45.7 ± 32.0	33.4 ± 23.4	18.3 ± 12.8	2.6 ± 1.8	0.8 ± 0.8
ZZ bkg	3.3 ± 1.6	6.9 ± 3.5	7.4 ± 3.7	7.0 ± 3.5	1.5 ± 0.8	0.4 ± 0.4
total bkg	82545 ± 24696	25672 ± 7571	1671 ± 380	298 ± 59	17.6 ± 3.9	3.1 ± 1.2
data	82228	25989	1758	?	?	?
significance	-0.0	0.0	0.2	?	?	?
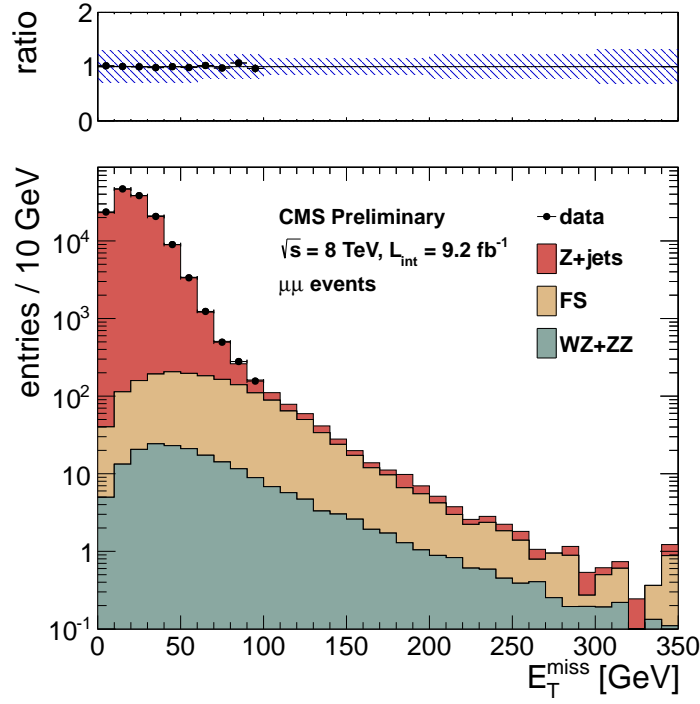
Figure 18: Results of the inclusive analysis in the $\mu\mu$ channel. The observed E_T^{miss} distribution (black points) is compared with the sum of the predicted E_T^{miss} distributions from $Z + \text{jets}$, flavor-symmetric backgrounds, and WZ+ZZ backgrounds. The ratio of observed to predicted yields in each bin is indicated. The error bars indicate the statistical uncertainty in the data and the shaded band indicates the total background uncertainty.

Table 17: Summary of results in the inclusive analysis in the $\mu\mu$ channel. The total background is the sum of the $Z + \text{jets}$ background predicted from the E_T^{miss} templates method ($Z + \text{jets}$ bkg), the flavor-symmetric background predicted from eμ events (FS bkg), and the WZ and ZZ backgrounds predicted from MC (WZ bkg and ZZ bkg). All uncertainties include both the statistical and systematic components. The Gaussian significance of the deviation between the data and total background is indicated for signal regions with at least 20 observed events.

	E_T^{miss} 0–30 GeV	E_T^{miss} 30–60 GeV	E_T^{miss} 60–100 GeV	E_T^{miss} 100–200 GeV	E_T^{miss} 200–300 GeV	E_T^{miss} > 300 GeV
$Z + \text{jets}$ bkg	107828 ± 32350	32794 ± 9840	1541 ± 465	68.3 ± 27.7	4.1 ± 1.3	0.7 ± 0.3
FS bkg	274 ± 51	526 ± 98	545 ± 102	279 ± 52	13.1 ± 4.2	1.7 ± 1.1
WZ bkg	34.5 ± 24.2	59.1 ± 41.4	42.0 ± 29.4	22.9 ± 16.1	3.1 ± 2.2	0.8 ± 0.8
ZZ bkg	4.3 ± 2.2	9.2 ± 4.6	10.0 ± 5.0	9.2 ± 4.6	1.7 ± 0.9	0.6 ± 0.6
total bkg	108140 ± 32350	33389 ± 9841	2138 ± 477	380 ± 61	22.0 ± 5.0	3.8 ± 1.5
data	108565	32964	2163	?	?	?
significance	0.0	-0.0	0.1	?	?	?

27

The E_T^{miss} distributions in the targeted analysis for the ee channel are displayed in Fig. 19 and the signal region yields are presented in Table 18. The E_T^{miss} distributions in the inclusive analysis for the $\mu\mu$ channel are displayed in Fig. 20 and the signal region yields are presented in Table 19.

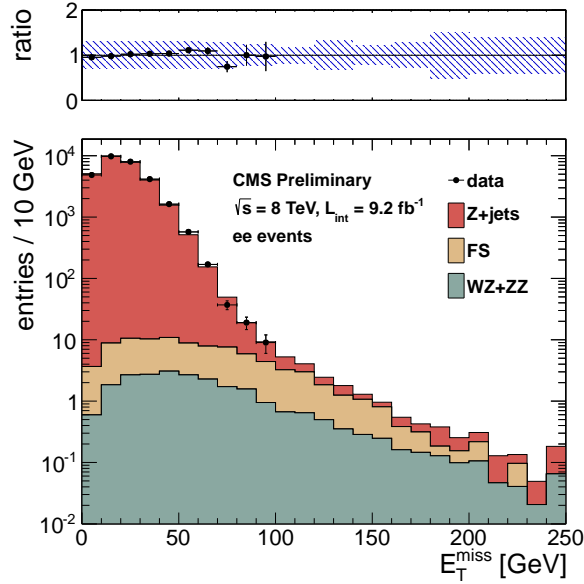Figure 19: Results of the targeted analysis in the ee channel. The observed E_T^{miss} distribution (black points) is compared with the sum of the predicted E_T^{miss} distributions from $Z+$jets , flavor-symmetric backgrounds, and WZ+ZZ backgrounds. The ratio of observed to predicted yields in each bin is indicated. The error bars indicate the statistical uncertainty in the data and the shaded band indicates the total background uncertainty.

Table 18: Summary of results in the targeted analysis in the ee channel. The total background is the sum of the $Z+$jets background predicted from the E_T^{miss} templates method ($Z+$jets bkg), the flavor-symmetric background predicted from eμ events (FS bkg), and the WZ and ZZ backgrounds predicted from MC (WZ bkg and ZZ bkg). All uncertainties include both the statistical and systematic components. The Gaussian significance of the deviation between the data and total background is indicated for signal regions with at least 20 observed events.

	E_T^{miss} 0–30 GeV	E_T^{miss} 30–60 GeV	E_T^{miss} 60–80 GeV	E_T^{miss} 80–100 GeV	E_T^{miss} 100–120 GeV
$Z+$jets bkg	22807 ± 6843	6065 ± 1820	188 ± 57	17.9 ± 6.2	3.1 ± 1.1
FS bkg	17.9 ± 3.6	21.5 ± 4.3	11.5 ± 2.4	7.8 ± 1.7	4.9 ± 1.1
WZ bkg	4.2 ± 2.9	6.8 ± 4.7	3.0 ± 2.1	1.8 ± 1.2	0.9 ± 0.6
ZZ bkg	1.0 ± 0.5	1.7 ± 0.9	1.0 ± 0.5	0.8 ± 0.4	0.4 ± 0.2
total bkg	22830 ± 6843	6095 ± 1820	204 ± 58	28.2 ± 6.5	9.3 ± 1.7
data	22581	6344	206	28	?
significance	-0.0	0.1	0.0	-0.0	?

	E_T^{miss} 120–140 GeV	E_T^{miss} 140–160 GeV	E_T^{miss} 160–180 GeV	E_T^{miss} 180–200 GeV	$E_T^{miss} > 200$ GeV
$Z+$jets bkg	1.2 ± 2.4	0.4 ± 0.1	0.3 ± 0.1	0.3 ± 1.0	0.4 ± 0.1
FS bkg	2.2 ± 0.6	1.3 ± 0.4	0.4 ± 0.2	0.1 ± 0.1	0.2 ± 0.1
WZ bkg	0.5 ± 0.4	0.3 ± 0.2	0.1 ± 0.1	0.1 ± 0.1	0.2 ± 0.2
ZZ bkg	0.3 ± 0.2	0.2 ± 0.1	0.2 ± 0.1	0.1 ± 0.1	0.3 ± 0.3
total bkg	4.2 ± 2.5	2.3 ± 0.5	1.0 ± 0.3	0.6 ± 1.0	1.0 ± 0.4
data	?	?	?	?	?
significance	?	?	?	?	?

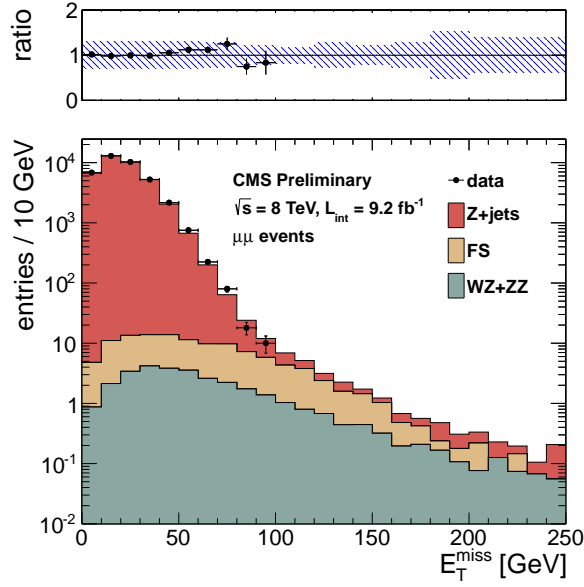Figure 20: Results of the targeted analysis in the $\mu\mu$ channel. The observed E_T^{miss} distribution (black points) is compared with the sum of the predicted E_T^{miss} distributions from $Z + \text{jets}$, flavor-symmetric backgrounds, and WZ+ZZ backgrounds. The ratio of observed to predicted yields in each bin is indicated. The error bars indicate the statistical uncertainty in the data and the shaded band indicates the total background uncertainty.

Table 19: Summary of results in the targeted analysis in the $\mu\mu$ channel. The total background is the sum of the $Z + \text{jets}$ background predicted from the E_T^{miss} templates method ($Z + \text{jets}$ bkg), the flavor-symmetric background predicted from eμ events (FS bkg), and the WZ and ZZ backgrounds predicted from MC (WZ bkg and ZZ bkg). All uncertainties include both the statistical and systematic components. The Gaussian significance of the deviation between the data and total background is indicated for signal regions with at least 20 observed events.

	E_T^{miss} 0–30 GeV	E_T^{miss} 30–60 GeV	E_T^{miss} 60–80 GeV	E_T^{miss} 80–100 GeV	E_T^{miss} 100–120 GeV
$Z + \text{jets}$ bkg	30017 ± 9005	7950 ± 2385	245 ± 74	23.0 ± 7.2	3.9 ± 1.2
FS bkg	23.0 ± 4.7	27.5 ± 5.6	14.7 ± 3.0	9.9 ± 2.1	6.3 ± 1.4
WZ bkg	5.3 ± 3.7	9.2 ± 6.4	3.6 ± 2.5	2.1 ± 1.5	1.2 ± 0.9
ZZ bkg	1.1 ± 0.6	2.4 ± 1.2	1.2 ± 0.6	1.0 ± 0.5	0.6 ± 0.3
total bkg	30047 ± 9005	7989 ± 2386	264 ± 74	36.0 ± 7.6	12.1 ± 2.1
data	29904	8132	304	28	?
significance	-0.0	0.1	0.5	-0.9	?
	E_T^{miss} 120–140 GeV	E_T^{miss} 140–160 GeV	E_T^{miss} 160–180 GeV	E_T^{miss} 180–200 GeV	E_T^{miss} > 200 GeV
$Z + \text{jets}$ bkg	1.4 ± 1.2	0.5 ± 0.1	0.3 ± 0.1	0.4 ± 0.5	0.5 ± 0.1
FS bkg	2.9 ± 0.7	1.7 ± 0.5	0.5 ± 0.3	0.1 ± 0.1	0.2 ± 0.2
WZ bkg	0.6 ± 0.4	0.5 ± 0.3	0.2 ± 0.1	0.2 ± 0.1	0.3 ± 0.3
ZZ bkg	0.5 ± 0.3	0.3 ± 0.2	0.2 ± 0.1	0.1 ± 0.1	0.4 ± 0.4
total bkg	5.4 ± 1.5	3.0 ± 0.6	1.2 ± 0.3	0.8 ± 0.5	1.3 ± 0.5
data	?	?	?	?	?
significance	?	?	?	?	?

C E_T^{miss} Templates from $\gamma + \text{jets}$ Sample

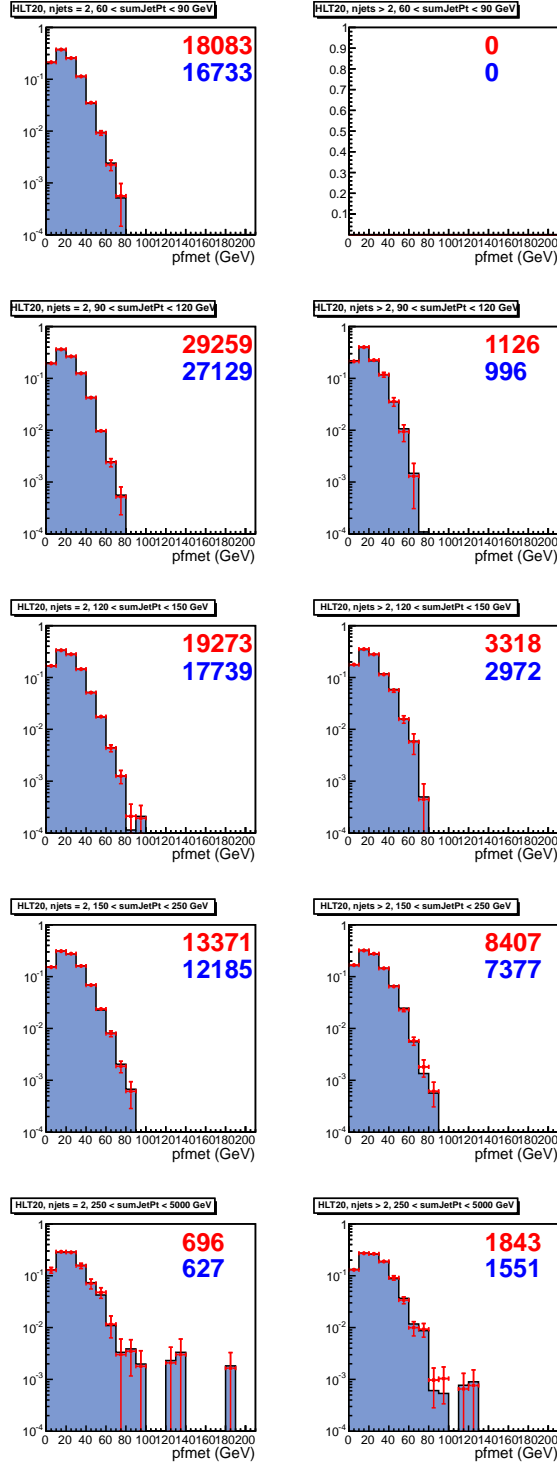In this section we display the templates used for the inclusive analysis (red) and the targeted analysis (blue).

Figure 21: E_T^{miss} templates collected with the $p_T > 22$ GeV single photon trigger. The number in red (blue) indicates the number of entries in the template for the inclusive (targeted) analysis.
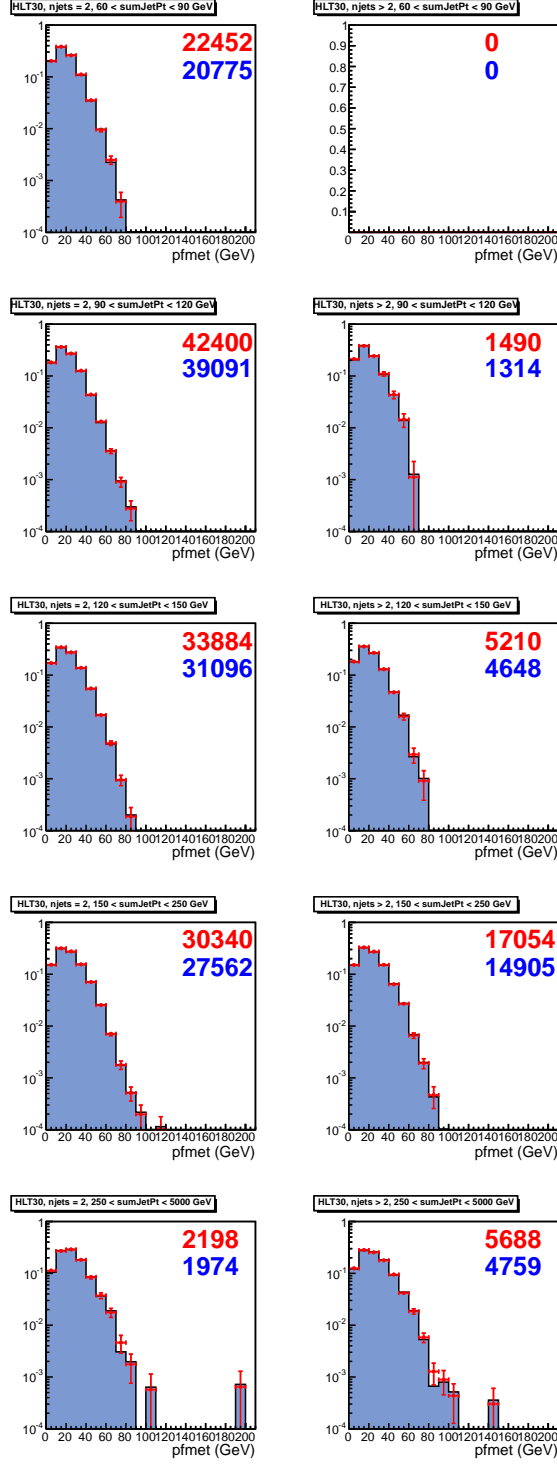
Figure 22: E_T^{miss} templates collected with the $p_T > 36$ GeV single photon trigger. The number in red (blue) indicates the number of entries in the template for the inclusive (targeted) analysis.
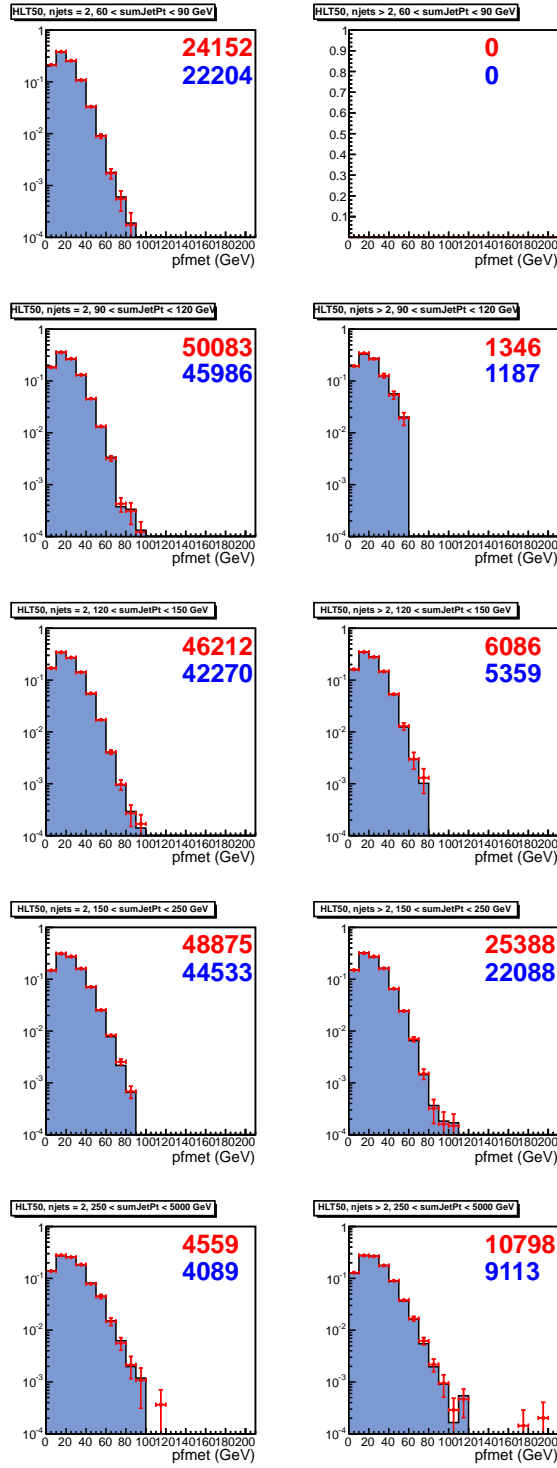
Figure 23: E_T^{miss} templates collected with the $p_T > 50$ GeV single photon trigger. The number in red (blue) indicates the number of entries in the template for the inclusive (targeted) analysis.
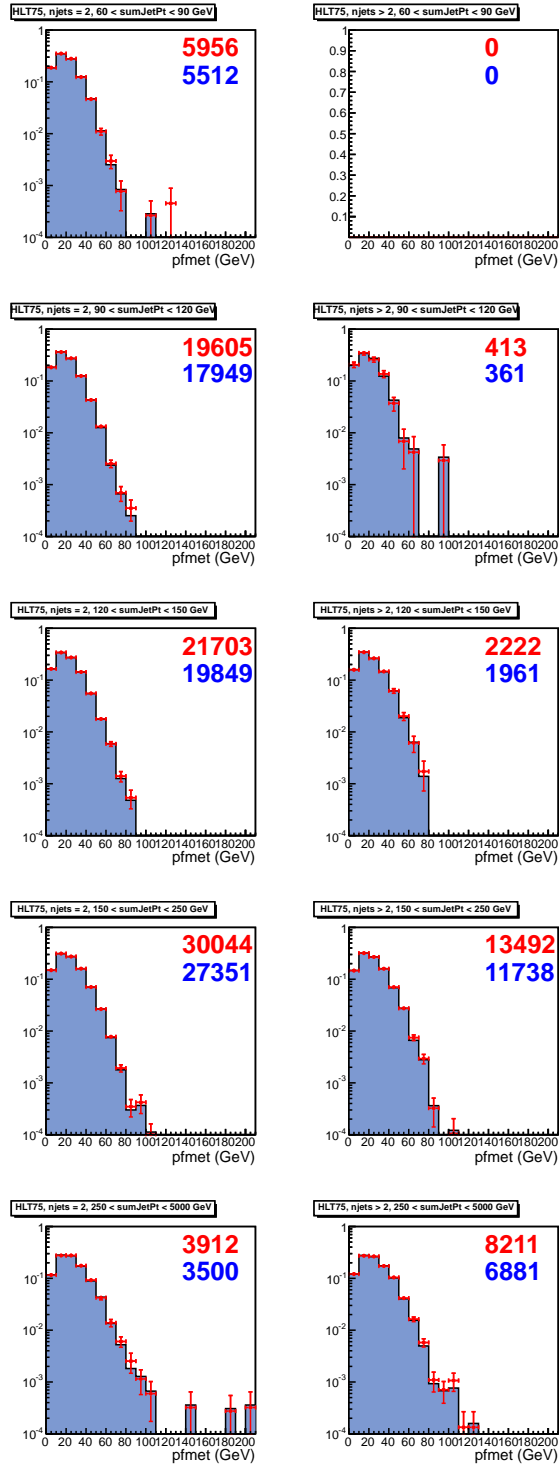
Figure 24: E_T^{miss} templates collected with the $p_T > 75$ GeV single photon trigger. The number in red (blue) indicates the number of entries in the template for the inclusive (targeted) analysis.
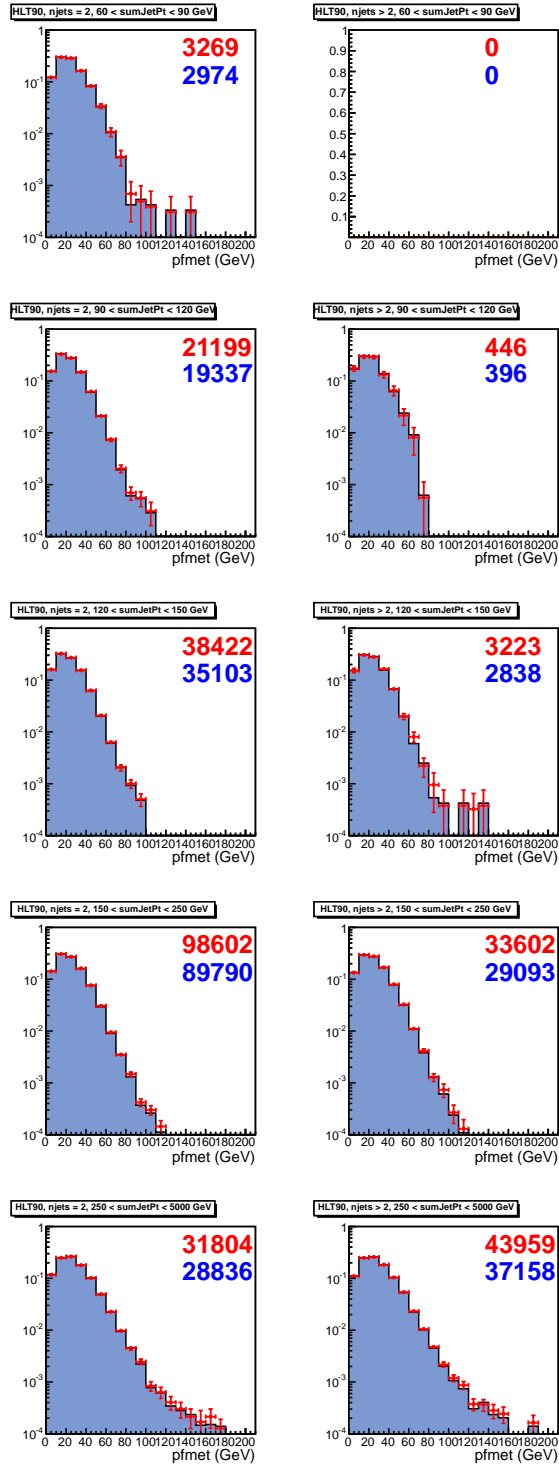
Figure 25: E_T^{miss} templates collected with the $p_T > 90$ GeV single photon trigger. The number in red (blue) indicates the number of entries in the template for the inclusive (targeted) analysis.